POLITECNICO DI TORINO

Faculty of Engineering

Master of Science in Mathematical Engineering

Master Thesis

A Finite Fracture Mechanics approach to brittle failure of adhesive lap joints

Advisors:
Prof. Pietro Cornetti
Prof. Wilfried Becker
Prof. Pierluigi Colombi

Candidate:
Giada Risso

July 2018

Acknowledgements

A special thanks to Professor Pietro Cornetti for helping me realizing his project and giving me an excellent support.

I would also like to say thanks to Professor Wilfried Becker for receiving me as a guest at the Technischen Universität Darmstadt and to Philipp Rosendahl and Julian Felger for the constructive discussions during my stay in Darmstadt.

Thanks to Mamma and Papá for always encouraging and supporting me, to Alex for all the afternoons spent together. To my classmates Domenica, Alessandro, Mattia, Luca and Michele for sharing this experience and a lot more. Thanks to Giada for our travelling; to Naomi, Adele and Michela for being on my side since ever; to Valentina for the laughs; to Sara for listening and to Michele for the music. Thanks to Konstantin for all the adventures together.

A final thanks goes to Politecnico di Torino and to all the people that are working for making the university a place where students can find their way through their future.

Summary

In this work a Finite Fracture Mechanics approach for predicting the load causing delamination along an interface of adhesive lap joints is presented. Beside the fact that the procedure used is general, the details are given for double lap joint and balanced single lap joint configurations.

For both geometries the failure load is predicted and compared with the solution given by other approaches such as the Linear Elastic Fracture Mechanics and Maximum Shear Stress Criterion. Regarding the double lap joint, a comparison with the widely-spread Cohesive Crack Model has been performed and the results found are almost coincident. This ensures that, for the study of the critical load, the used approach gives reliable predictions and, due to its simplicity, is advantageous with respect to the more complex Cohesive Crack Model. The predictions have been validated also against experimental results for both geometries.

A particular focus has been performed on the two different hypotheses that crack can propagate from one or from both sides of the adhesive region. This investigation shows interesting results especially for what concerns the Double Lap Joint configuration, where the predicted critical load for allowing crack propagation on both sides is lower than the one predicted by assuming that the crack propagates only on side. Moreover, the discontinuity between those two predictions depends on the symmetry of the considered geometry. For the Single Lap Joint instead these different hypotheses are not affecting the results.

The failure behaviour described by the combination of stress and energy criterion, which allows one to have an agreement with experimental results and to highlight the effects of geometrical parameters, requires only basic failure parameters and can be computed on a personal computer.

Contents

Chapter 1

Introduction

1.1 Motivations

The use of adhesives has increased considerably in the last decades due to the advantages against other assembly techniques. Adhesive bonds allow almost any unequal material to be joined without weakening the structures. Especially for multiple joining of thin-walled structures, adhesive bonds with modern polymer adhesives can be used very advantageously. Without a detailed understanding of failure processes and reliable methods for predicting the failure loads, costly and expensive design experiments are necessary.

In industrial practice, the design of any adhesive bonded structure requires theoretical studies to predict critical load and ensure reliability of the structure. One well known example can be given from the aviation industry: the performance of adhesive bonded components has varied significantly in recent history and the adhesive bonding resulted not to be reliable; due to this fact, adhesive bond failures require closer scrutiny to accurately assess the causes of these failures [13]. The knowledge that is needed in order to entirely understand the properties and behavior of bonded joints is immense and several models for predicting critical loads have been presented in the past. For this reasons it is important to develop a quick and efficient evaluation of the failure load.

1.2 Goal of the studies

The aim of this work is the development of efficient methods for evaluating adhesive bonds. For real structures several different configurations exist; due to their importance, the presented study is applied to the Single Lap Joint configuration (Figure 1.1) and to the Double Lap Joint (Figure 1.2). Even though the geometry is simple, the mechanical behaviour and failure mechanisms of those adhesive joints are very complex because of the presence of singularities in the stress configurations at the junction between adherent and adhesive.

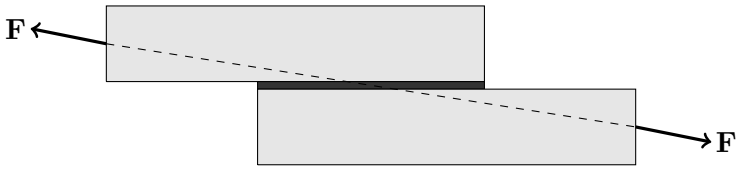

Figure 1.1: Single Lap Joint configuration

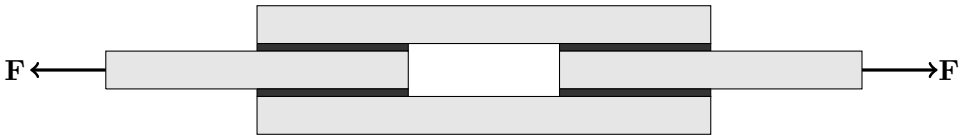

Figure 1.2: Double Lap Joint configuration

The failure of adhesive bonds often occurs by initiation of cracks at the edge of the adhesive layer. Bypassing the presence of stress singularities, it has been used a simple beam model to achieve the stress field. Crack initiation is then investigated with a coupled stress and energy criterion in the context of finite fracture mechanics.

In different finite fracture mechanics approaches (e.g. [19], [18]) applied to the geometries that have been studied, the crack propagation is supposed to start only from one of the two edges of the adhesive. One aim of this work is to study the problem illustrated with an efficient implementation of the coupled criterion supposing that crack propagation can start from both extremes of the junction. The failure load predictions of the developed models have been compared with failure loads determined experimentally in order to assess the quality of the analysis presented. A deep comparison on the differences of critical loads obtained with a model that predicts crack propagation only on one side and from both has been performed for the double lap joint. Then the analysis has been done on the single lap joint for the specific case of equal heights of the adherents (balanced joints). Note that it will be clarified later that the symmetric single lap joint geometry is the more interesting one for investigating the need or not of the supposition of double crack-side initialization and propagation.

1.3 Structure of the work

In Chapter 2 a summary of the theoretical background is given: fracture mechanics fundamentals, strength criteria, energy criteria and finally a presentation of the Finite Fracture Mechanics (FFM) approach. Linear elasticity is supposed to be already known by the reader.
Chapter 3 is presenting the study performed on the Double Lap Joint (DLJ) configuration; starting with the illustration of the evaluation of stress at the interface, then showing the coupled criterion under several different hypotheses.

In Chapter 4 the Single Lap Joint (SLJ) symmetric configuration is investigated. The chapter is structured as the DLJ one with the difference that two different models for the stresses at the interface are presented.
A presentation of the results on both joint configurations is then illustrated in Chapter 5. In this section a parametric analysis and comparison with different experimental results is shown in order to perform a critical analysis on the proposed method.
The work ends, at Chapter 6, with general conclusions and suggestions on how the study could be continued.

Chapter 2

Theoretical Background

In the following chapter the theoretical background needed for this work is summarized. In particular, the fundamentals of finite fracture mechanics and coupled stress and energy criteria are introduced. Throughout the whole work a uniform notation is used that will be herein introduced.

2.1 Strength criteria

The mechanical behavior of deformable bodies with linear elastic material behavior is described by the linear elasticity theory. It is used as a starting point for theories of solid mechanics.
To describe the failure of materials and structures, strength criteria were introduced at the end of the 19^{th} century. In this case, a function of the stresses is defined and compared with a critical value. This critical value is often called strength. The failure condition is:

$$f(\sigma) = \sigma_c$$

where f is a general function of the stresses. This condition can be represented as a failure surface in the three-dimensional space of the principal stresses.
There are several strength criteria that have been presented and each of them performs best for its specified constraints. For example, Rankine's stress criterion assumes that failure occurs in a brittle body when the maximum normal stress reaches a critical value:

$$\sigma_{max} = \sigma_c$$

This strength criterion is typically used to describe failure in brittle materials.
Another example is von Mises yield criterion, also called maximum distortion energy criterion: it can be also formulated in terms of the von Mises stress or equivalent tensile stress $f(\sigma) = \sigma_{eq}$. This is a scalar value of stress that can be computed from the Cauchy stress tensor. Supposing this case a material starts to yield when the von Mises stress reaches a value known as yield strength σ_c. For materials under multi axial loading conditions, being at a principal stress configuration, σ_{eq} is given by:

$$\sigma_{eq} = \sqrt{\frac{1}{2}((\sigma_1 - \sigma_2)^2 + (\sigma_2 - \sigma_3)^2 + (\sigma_3 - \sigma_1)^2)}$$

This criterion is used in many areas of engineering, especially in the study of plastic material behavior.
The following failure criterion is known as Maximum Shear Stress Criterion (MSSC) or Tresca criterion. This theory postulates that failure will occur when the maximum shear stress exceeds a threshold value. For materials under multi axial loading conditions, being in a principal stress configuration, σ_{eq} is given by:

$$\sigma_{eq} = \max\{|\sigma_1 - \sigma_2|, |\sigma_2 - \sigma_3|, |\sigma_3 - \sigma_1|\}$$

In the following section the fracture mechanics theory will be introduced.

2.2 Fracture mechanics

Fracture mechanics deals with the analysis of cracks, their formation and propagation. Compared to strength approaches, it is relatively young. There were no developments until the beginning of the 20^{th} century. Griffith published in 1921 his reflections on energetic considerations of failure [9] after performing himself some experiments on glass fibers that suggested that a new approach was needed in order to explain the failure of brittle materials. This was first picked up by Irwin (1957) [12] and thus laid the foundation stone of fracture mechanics.

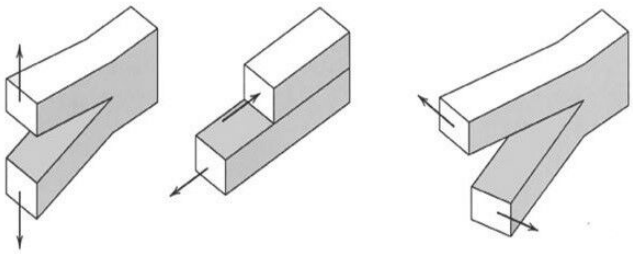

Figure 2.1: From left to right: Mode I , Mode II and Mode III crack opening

The base of fracture mechanics is the Linear Elastic Fracture Mechanics (LEFM). It is assumed that only very locally in a plastic zone at crack tip inelastic processes occurs and it is found that such failures always originate at some type of crack or flaw.

2.2.1 Linear Elastic Fracture Mechanics

Linear Elastic Fracture Mechanics makes use of the elastic stress analysis to define the conditions under which the existing crack will extend. The basic assumptions are the same as the ones of the strength of materials theory: the material is a homogeneous isotropic

continuum, stress is proportional to strain.
In this theory, a distinction is generally made between three different crack-opening modes showed in Figure 2.1, where Mode I indicates the opening of a crack normal to its banks of cracks; Mode II is the tangential shift of the crack edges in the plane normal to the crack front and Mode III is the tangential displacement of the crack edges tangential to the crack front. The case of superposition of these crack-opening modes, is named mixed-mode loading. Finally, considering that fracture is usually a very irregular process on a microscopic scale, in fracture mechanics only the macroscopic mode of crack growth is considered.

2.2.2 Griffith approach

The introduction of an energy criterion in the study of the development of fractures was made by Griffith (1920). Note that, before Griffith, progress toward a quantitative definition of toughness began with the work of Inglis in 1913 [11]. He showed that the local stresses around a hole in a stressed plate are higher than the average applied stress. With his results he showed that the degree of stress concentration at the edge of the hole depends on the radius of curvature of the hole and then he analyzed the limit case of a narrow elliptical hole. One of the reason why Griffith looked for a new approach is that, contrary to the well known fact that larger cracks are propagating more easily than smaller ones, the solution of Inglis was not depending on the absolute size of the crack.

The idea of Griffith starts with a theoretical analysis of fracture propagating based on the energy needed for a crack growth. According to Griffith, the necessary condition for crack growth is that the amount of strain energy released must be greater or equal to the energy required for the new crack faces to be created. That can be expressed:

$$\frac{dU_s}{da} \geq \frac{dU_\gamma}{da} \tag{2.1}$$

where U_s is the strain energy, U_γ is the surface energy, and da is the crack length increment; we will call a the pre existing crack length. Then Griffith proceeded with using Inglis's stress field solution for a narrow elliptical crack of length $2a$ to show that the strain energy released and the surface energy in an infinite plate under a uniformly remote applied stress σ_{ext} are given by:

$$\begin{aligned} U_s &= \frac{\pi a^2 \sigma_{ext}^2}{E} \\ U_\gamma &= 4a\gamma \end{aligned}$$

where γ is the fracture surface energy of the solid and E is the Young modulus. Note that this is the solution for case of plane stress; for cases of plane strain E has to be replaced by $\frac{E}{(1-\nu^2)}$, where ν is the Poisson's ratio.
Applying the inequalities expressed in 2.1 shows that strain energy release rate per increment of crack length is a linear function of crack length.

$$\frac{\pi a \sigma_{ext}^2}{E} \geq 2\gamma \tag{2.2}$$

Note that this energy balance indicates whether crack growth is possible, but that it will occur depending on the configuration of stress at the crack tip. In other words, if, for example, the crack tip is rounded, then the crack may not grow because of an insufficient stress concentration. So the crack tip has to be loaded to the tensile strength.

Usually the criterion is expressed by the following formulation:

$$G = \left[\frac{dU_s}{da}\right]_{P=cost} = -\left[\frac{dU_s}{da}\right]_{u=cost} \geq G_c \tag{2.3}$$

where G is called strain energy release rate and can be evaluated by either considering that external load P or the displacement u is maintained constant. G_c is called the fracture energy or critical energy release rate and is a material property. dA is the infinitesimal crack area that is da multiplied by the width t.

2.2.3 Irwin's relationship

Moreover, Williams (1952) [20] introduced the stress intensity factor K that depends on the geometry, the size, the location of the crack and the loading mode. Accordingly the asymptotic stress field at the crack tip vicinity (in mode I) becomes:

$$\sigma_{i,j}(r,\theta) = \frac{K_I}{\sqrt{2\pi r}} f_{i,j}(\theta) \tag{2.4}$$

where higher order terms have not been reported in the right-hand side and $\sigma_{i,j}$ is the stress distribution close to the crack tip, the polar coordinate system (r,θ) has the origin where at the crack tip and $f_{i,j}(\theta)$ is the angular function. In general, K can be found in handbooks or computed numerically. This factor, for the example of straight crack with a length of $2a$ perpendicular to the loading direction presented before is:

$$K_I = \sigma_{ext}\sqrt{\pi a} \tag{2.5}$$

In case of linear elasticity, Irwin (1957) [12] demonstrated that there is a relation between the strain energy release rate and the stress intensity factor that, for a crack under mode I loading, is:

$$G = \frac{K_I^2}{E'} \tag{2.6}$$

where

$$E' = E \text{ for plane stress}$$
$$E' = \frac{E}{1-\nu^2} \text{ for plane strain}$$

thus the criterion expressed in Equation 2.3 for a crack under mode I loading is equivalent to:

$$K_I = K_{Ic} \tag{2.7}$$

The Mode I critical stress intensity factor, K_{Ic} named fracture toughness, is the most often used engineering design parameter in fracture mechanics.
So, according to LEFM, it is not necessary to know the whole stress field but only the stress intensity factor.
Related to the problem that theoretically the stress singularity is present at the crack tip whereas this is not possible in real applications, the stress at the crack tip is limited to at least the yield strength of the material. Thus, the region called *crack tip plastic zone* is defined as the non linear region where linear elasticity cannot be assumed. In other words, a certain distance of the crack tip has to be assumed. For this reason LEFM can only be applied if specified constraints over the material proprieties of the solid are satisfied.

2.3 Cohesive Crack Model

This method is quickly introduced now because the two cohesive laws that will be presented can be related to the application of the coupled criterion explained in Section 2.5. According to the fact that there are problems arising while applying the LEFM due to stress singularities for particular geometries, such as short cracks or V-Notches, a solution has been presented by Hillerborg et al. (1976) with the so called Cohesive Crack Model (CCM) [10]. This is a well-established model with a clear physical background and that gives very accurate predictions, with the disadvantage that is computationally expensive. Moreover, for sufficiently large cracks, CCM provides the same results of LEFM and is suitable for brittle and quasi-brittle materials. Figure 2.2 illustrates a typical situation of crack tip.
In the region close to the crack tip, by using the parameter a_p, a process zone is defined.

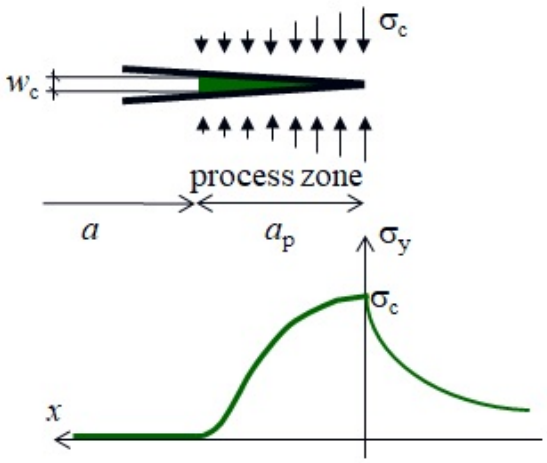

Figure 2.2: Scheme of the process zone around a crack tip.

The left extreme represents the real crack tip and the right extreme the fictitious tip. The

idea is then to define a cohesive law that describes the mechanical behaviour at the interface in the transaction region, depending on the crack opening length w. Note that the real crack tip corresponds to the point where w reaches a critical value w_c that depends on the material. Two different relationships are given by the so called Dudgale cohesive law

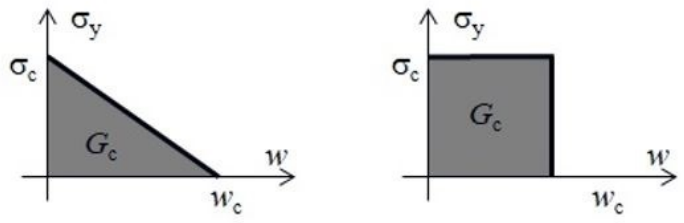

Figure 2.3: Cohesive laws: on the left side the linear softening and on the right Dudgale's law

and the linear softening cohesive law. The Dudgale shape for the cohesive law states that the stress is constant and equal to σ_c as long as the crack opening w reaches the value w_c, while the linear softening states that the stress linear decreases from σ_c to 0 in the interval $[0, w_c]$ The two laws are shown in Figure 2.3. The area under the cohesive law corresponds to the fracture energy G_c and the ductile behaviour is described by $\sigma_c \to 0$ and $w_c \to \infty$. The fact that this is computationally expensive is a consequence of the order of magnitude of a_p that is typically very small with respect to the structural size.

2.4 Non-local stress criteria

Other methods has been presented for avoiding the problems of the LEFM mentioned above. In this section the average stress criterion and the Leguillon's (or Point method) are introduced. In order to have a simple example, both formulation refers to the situation illustrated in Figure 2.4

- **Average stress criterion**
  This method was proposed by Novozhilov in the 1969 [16] assuming that crack can propagates only of a finite jump Δ and the stress criterion can be written in the following formulation:
  $$\frac{1}{\Delta}\int_0^{\Delta} \sigma_y(x)\mathrm{d}x \geq \sigma_c \tag{2.8}$$
  With this formulation, even though the stresses close to the crack tip have a singularity, the approximation given by the average integral is a finite quantity.

- **Point Method**
  This approach assumes that crack can propagates only of a finite jump Δ but the

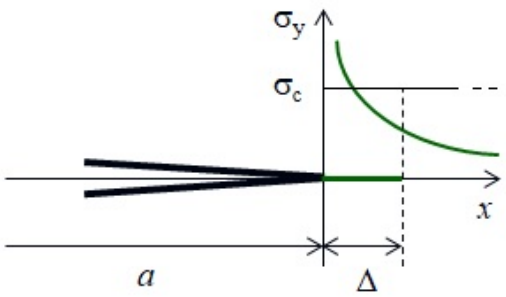

Figure 2.4: Representation of the stress configuration at crack tip

stress criterion is applied with the following formulation that is well explained by Leguillon (2002) [14]:

$$\sigma_y(x) \geq \sigma_c \text{ for all } x \in (0, \Delta) \tag{2.9}$$

That can be expressed as an equation in case the stress distribution is decreasing in the interval $(0, \Delta)$.

In both the previous criteria, Δ is a (constant) material propriety.

2.5 Finite Fracture Mechanics

2.5.1 General theory

The idea of Finite Fracture Mechanics (FFM) is based on a coupled stress and energy criterion. Supposing the critical load provides a discrete fracture, called Δ, the instantaneous formation of the finite size crack is predicted when a stress criterion and an energy criterion are both fulfilled. This method is young and has been presented and analyzed in the article by Leguillon (2002) [14] and in the article by Cornetti et al. (2006) [4].

The formation of the finite crack must meet Griffith's criterion of fracture. The released energy must therefore be greater than or equal to the energy required for the breakage. Or, equivalently, the energy criterion can be written by using the stress intensity factor. On the other hand, the crack to grow also need to fulfill the condition given by the stress criterion. This can be either formulated by using the average criterion or the Point Method criterion presented in the previous section. The two formulations can be written with the

following systems of inequalities:

$$\begin{cases} \int_a^{a+\Delta} \sigma(x,a)\mathrm{d}x \geq \sigma_c \Delta \\ \int_a^{a+\Delta} G(a')\mathrm{d}a' \geq G_c \Delta \end{cases} \tag{2.10}$$

$$\text{or} \quad \begin{cases} \sigma(x,a) \geq \sigma_c \quad \text{for all } x \in (a, a+\Delta) \\ \int_a^{a+\Delta} G(a')\mathrm{d}a' \geq G_c \Delta \end{cases} \tag{2.11}$$

Both systems are made of two equations in two unknowns: the external load that generates the propagation of the crack, that is called failure load F_c and the finite crack advancement Δ. Each inequality is a necessary condition for fracture to propagate but together they form a necessary and sufficient condition. In particular the energy balance provides a lower bound for crack advancement while the stress criterion the upper one. For low load level, the lower bound is larger than the upper bound: there is no solution and no crack propagation occurs but when the load increases the two crack propagation meets and the solution is found. In particular, for positive geometries, i.e. G monotonically increasing, the failure load is achieved when both inequalities are strictly fulfilled.
In this method the Δ is not a constant of the material but a structural parameter. For large cracks the results are in accordance with LEFM and, moreover, several results in accordance with the CCM have been found.
Some observations has been done regarding which of the two formulations is better to choose: in the article presented by Cornetti et al. (2014) [6], it is well explained how the results found by using FFM with the Leguillon's formulation for the stress criterion are more in accordance with the supposition of the Dudgale's cohesive law, while the average criterion with the linear softening.

$$\int_a^{a+\Delta} \sigma(x,a)\mathrm{d}x \geq \sigma_c \Delta \qquad \Longleftrightarrow \text{ Dudgale's cohesive law}$$

$$\sigma(x,a) \geq \sigma_c \quad \text{for all } x \in (a, a+\Delta) \qquad \Longleftrightarrow \text{ linear softening}$$

2.5.2 Formulation in this work

For the study of the single and double lap joint geometries, the weak interface model has been used for modelling the adhesive layer between two materials. By denoting with E_a, h_a, G_a the Young's modulus, the thickness of the adhesive and the shear modulus, the adhesive layer can been modeled as a bed of springs normal and tangent to the interface. Figure 2.5 schematize the model used in this specific work. The stiffness of the springs are $k_n = \frac{E_a}{h_a}$ for the normal and $k_t = \frac{G_a}{h_a}$ for the tangential ones.

In this specific work, after studying with the linear elastic theory the stresses configurations at the interface of the adhesive joints, the following formulations have been used in order to apply correctly Finite Fracture Mechanics.
The energetic condition is given by a linear interaction law of G_I and G_{II} that are the energies release rates respectively in pure mode I and II respect to their fracture toughness

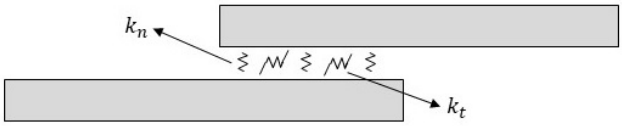

Figure 2.5: Representation of the weak interface

G_{Ic} and G_{IIc}. Moreover, it has been assumed for simplicity that $G_{IIc} = 2G_{Ic}$. In order to evaluate the strain energy release rate G in elastic interface geometries is not possible to use the Irwin's formulation given in Equation 2.6. Thus the formulation provided by Lenci (2001) [17] has been used: the strain energy release rate equals the strain energy stored in the spring ahead the crack tip:

$$G_I = \frac{\sigma_{max}^2}{2k_n} \quad \text{and} \quad G_{II} = \frac{\tau_{max}^2}{2k_t} \tag{2.12}$$

In case of delamination under pure mode II loading the FFM criterion reads:

$$\begin{cases} \int_a^{a+\Delta} \tau(x,a)\mathrm{d}x \geq \tau_c \Delta \\ \int_a^{a+\Delta} \frac{\tau_{max}(a')^2}{2k_t}\mathrm{d}a' \geq G_{IIc}\Delta \end{cases} \tag{2.13}$$

$$\text{or} \quad \begin{cases} \tau(x,a) \geq \tau_c \quad \text{for all } x \in (a, a+\Delta) \\ \int_a^{a+\Delta} \frac{\tau_{max}(a')^2}{2k_t}\mathrm{d}a' \geq G_{IIc}\Delta \end{cases} \tag{2.14}$$

While in case of mixed mode, the maximum normal stress criterion has been used in this formulation (as has been done by Stein et al. [18]). Accordingly, a combination of the adhesive shear and peel stresses is considered:

$$\sigma_s = \frac{\sigma_{max}}{2} + \sqrt{\left(\frac{\sigma_{max}}{2}\right)^2 + (\tau_{max})^2} \tag{2.15}$$

According to this definition the coupled criterion can be expressed in the following way:

$$\begin{cases} \int_a^{a+\Delta} \sigma_s(x,a)\mathrm{d}x \geq \sigma_c \Delta \\ \dfrac{\int_a^{a+\Delta} \frac{\tau_{max}(a')^2}{2k_t}\mathrm{d}a'}{2G_{Ic}} + \dfrac{\int_a^{a+\Delta} \frac{\sigma_{max}(a')^2}{2k_t}\mathrm{d}a'}{G_{Ic}} \geq \Delta \end{cases} \tag{2.16}$$

$$\text{or} \quad \begin{cases} \sigma_s(x,a) \geq \sigma_c \quad \text{for all } x \in (a, a+\Delta) \\ \dfrac{\int_a^{a+\Delta} \frac{\tau_{max}(a')^2}{2k_t}\mathrm{d}a'}{2G_{Ic}} + \dfrac{\int_a^{a+\Delta} \frac{\sigma_{max}(a')^2}{2k_t}\mathrm{d}a'}{G_{Ic}} \geq \Delta \end{cases} \tag{2.17}$$

Both formulations with the average stress or Leguillon have been tested for the Double Lap Joint geometry, while for the Single Lap Joint the average formulation has been preferred. In case of monotonically decreasing stress in the region close to the stress singularity and increasing energy release rate the two inequalities can be replaced by two equations. The failure load F_c can be defined as the minimum load that satisfied both conditions. In the study of the Double Lap Joint illustrated in the next chapter, it has been possible to decouple the inequalities and obtaining an implicit non linear equation for the crack length Δ. In other words, it has been possible to define the critical load $F_{c,e}(\Delta)$, $F_{c,s,a}(\Delta)$ and $F_{c,s,L}(\Delta)$ that are respectively the critical load given by the energy criterion, the average stress criterion and the Leguillon's formulation for the stress criterion.
In this specific case, applying the FFM means that the F_c is found in the following way:

$$\begin{aligned} F_c = &\min_{F,\Delta} F \\ &\texttt{subject to}: \\ &F \geq F_{c,e}(\Delta) \\ &F \geq F_{c,s,*}(\Delta) \quad \text{with * equal to } a \text{ or } L \end{aligned} \tag{2.18}$$

Unfortunately, obtaining the explicit linear formulation is not possible for the Single Lap Joint geometry and the problem can be express in the following way:

$$\begin{aligned} F_c = &\min_{F,\Delta} F \\ &\texttt{subject to}: \\ &\int_a^{a+\Delta} \sigma_s(x,a)\mathrm{d}x \geq \sigma_c \Delta \\ &\frac{\int_a^{a+\Delta} \frac{\tau_{max}(a')^2}{2k_t}\mathrm{d}a'}{2G_{Ic}} + \frac{\int_a^{a+\Delta} \frac{\sigma_{max}(a')^2}{2k_t}\mathrm{d}a'}{G_{Ic}} \geq \Delta \end{aligned} \tag{2.19}$$

where the σ_s, τ_{max} and σ_{max} depend on the load F.

Chapter 3

Double Lap Joint

In the following chapter the double lap joint configuration will be investigated with the tools illustrated in Chapter 2. Firstly the study of the interface stresses is presented, then the critical load will be studied with the coupled criterion.

3.1 Description of the model

As is shown in Figure 3.1, the double lap joint configuration considered herein is symmetric with respect to the mid plane of the inner adherent: i.e. the two outer plates are equal. However, the material of the inner adherent may be different from the material of the outer plates. The joint is also symmetric with respect to the plane situated at mid length of the unbonded central part and orthogonal to the plates. Taking advantage of this double symmetry, only one quarter of the joint is considered for modelling. The geometrical parameters that describe the joint are shown in the just mentioned figure. The index r indicates the reinforcements (i.e. outer adherents), the index b the block in the middle and the index a indicates the adhesive; the width of the geometry is defined by the quantity t. Note that this geometry refers to a model where the adherents are considered as a bed of tangential springs. If both tangential and normal springs are considered, an external momentum has to be taken into account at the right hand side of the outer adherents.

The following main assumptions have been done:

- the adherents are modelled as Timoshenko beams;
- the adhesive is modelled as a spring bed transmitting either only shear stress or peel and shear stresses, whose values are assumed to be representative of the stresses in the mid-thickness plane of the layer, the remaining stress components in the adhesive are neglected;
- the mechanisms of deformability of the adherents due to the adhesive peel and shear stresses are included into the model by properly setting the spring stiffness modelling the adhesive.

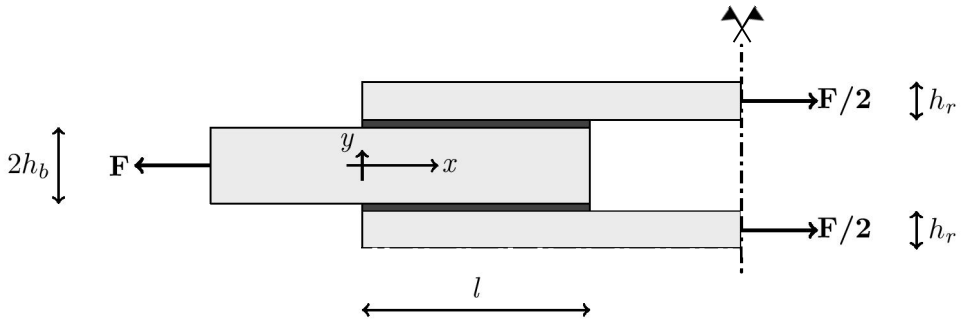

Figure 3.1: Half of the Double Lap Joint geometry

In the following section it will be presented how to derive the model equations in the case only shear stress is considered for modelling the adhesive.

3.2 Shear lag model

In this section the adhesive is modelled as a bed of springs and the peel stress is ignored.

3.2.1 Derivation of the shear stress

Figure 3.2 is showing an infinitesimal section of the overlap region of the geometry.

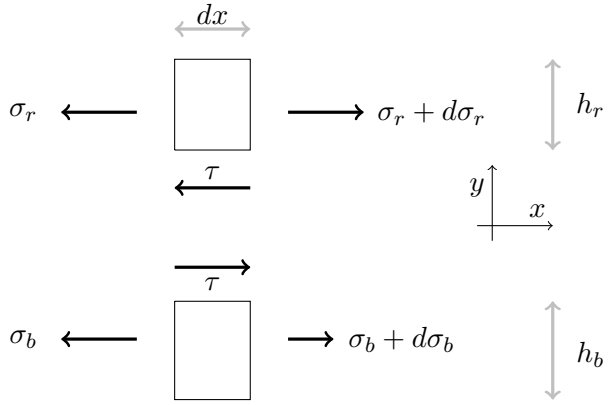

Figure 3.2: Infinitesimal section of the overlap region

Referring to the free body diagram the following equations can be written:

$$\sigma_r h_r t_r + \sigma_b h_b t_b = \frac{F}{2} \tag{3.1a}$$

$$h_r \frac{d\sigma_r}{dx} - \tau = 0 \tag{3.1b}$$

Calling the longitudinal displacement of the reinforcements and the block respectively u_r and u_b, and introducing the difference of the displacements:

$$s = u_r - u_s$$

taking into account that the adhesive is modelled as a spring bed, and the Timoshenko beam kinematic assumption, it can be written that:

$$\tau = k_t s \tag{3.2}$$

where k_t, the tangential stiffness, is given by:

$$k_t = \frac{G_a}{h_a}$$

and the shear elastic modulus and the thickness of the adhesive are respectively called: G_a and h_a. Moreover the following constitutive equations are given as:

$$\sigma_r = E_r \frac{du_r}{dx} \tag{3.3a}$$

$$\sigma_b = E_b \frac{du_b}{dx} \tag{3.3b}$$

By writing σ_b as a function of σ_r from Equation 3.1a and applying basic mathematical steps, the following differential equation is derived:

$$\frac{d^2 s}{dx^2} - \frac{1 + \frac{E_r t_r h_r}{E_b t_b h_b}}{E_r h_r} k_t s = 0 \tag{3.4}$$

Those quantities are then introduced in order to perform non-dimensional analysis:

Characteristic length: $l_{ch} = \sqrt{\dfrac{E_r h_r}{k_t(1+\rho)}}$

Interface brittleness index: $\mu = \dfrac{2 k_t G_c}{\tau_c^2}$

this parameter is defined in order that if $\mu = 1$ this corresponds to a linear elastic perfectly brittle interface behaviour and $\mu \to \infty$ to a linear elastic perfectly plastic interface.

Mechanical fraction of the reinforcement: $\rho = \dfrac{E_r t_r h_r}{E_b t_b h_b}$

For an easier evaluation in the following calculations it will be supposed $\rho \leq 1$. The details for the case when $\rho > 1$ are shown in the Appendix B.

Defining:

$$\xi = \frac{x}{l_{ch}}, \quad \lambda = \frac{l}{l_{ch}}, \quad \delta = \frac{\Delta}{l_{ch}}, \quad \overline{\tau} = \frac{\tau}{\tau_c}, \quad \overline{F} = \frac{F}{F_c^{\infty}},$$

Where the F_c^{∞} is the failure load for infinite overlap length:

$$F_c^{\infty} = 2t_r\sqrt{2(1+\rho)E_r h_r G_c} \tag{3.5}$$

that can be found by using the energy criterion of the double lap joint configuration and supposing that the overlap length $l \to \infty$.

The quantities G_c and τ_c are the fracture energy and the shear strength and have already been introduced in the previous chapter.
The second order differential Equation 3.4 can be solved considering the boundary conditions:

$$\sigma_r = \frac{F}{2t_r h_r} \qquad \text{for: } x = l \tag{3.6a}$$

$$\sigma_r = 0 \qquad \text{for: } x = 0 \tag{3.6b}$$

Giving the following dimensionless expression for the shear stress:

$$\overline{\tau} = \overline{F}\sqrt{\mu}\,\frac{\rho\,\cosh(\lambda-\xi)+\cosh(\xi)}{\sinh(\lambda)} \tag{3.7}$$

Figure 3.3 shows an example of the shape of the shear stress in the interface for $\rho = 0.7$. Note that in case the double lap joint is symmetric (i.e. $\rho = 1$) the τ is symmetric.

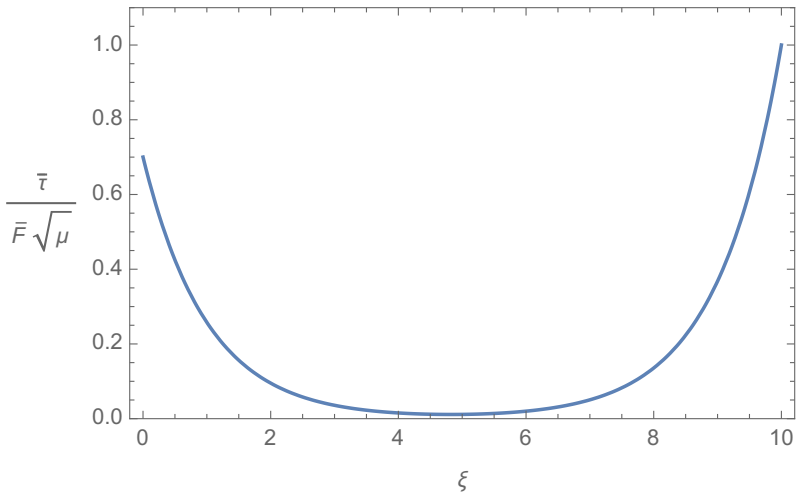

Figure 3.3: Plot of $\frac{\overline{\tau}}{\overline{F}\sqrt{\mu}}$ for $\rho = 0.7$ and $\lambda = 10$

The maximum values of the shear stress are at the edges of the overlap region. Moreover, if $\rho < 1$ the global maximum is in $\xi = \lambda$ (i.e. $x = l$), if $\rho > 1$ in $\xi = 0$, in the end for $\rho = 1$ the shear stress has the same maximum values at both edges.
This final observation is the reason why it has been studied that the crack propagation might be on both sides of the overlap region: the shear criterion is allowing crack propagation on both sides in case the critical shear stress is low enough for being lower than the shear stress at both extremes of the ξ domain.

3.2.2 Critical load

The coupled criteria is presented now by using Equation 3.7 previously given of the shear stress at the interface. Two different cases are considered:

- The crack propagates only on the side where the shear stress is higher: for $\rho < 1$, on the right (Figure:3.4);
- the crack propagates on both side of two different crack lengths (Figure:3.6).

Crack propagation only on the right side

Figure 3.4 schematizes a quarter of the geometry of the double lap joint.

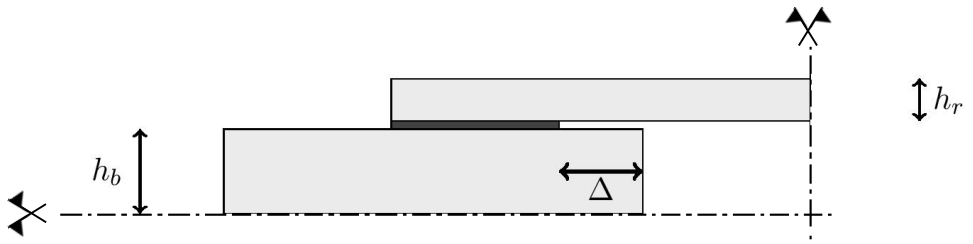

Figure 3.4: Crack propagation only on the right side

Calling Δ the finite crack advance, we introduce the following dimensionless quantity:

$$\delta = \frac{\Delta}{l_{ch}}$$

- **Energy criterion**

  In this specific case applying the energy criterion means:

$$l_{ch} \int_{\lambda-\delta}^{\lambda} \frac{\tau_{max}^2(\overline{\lambda})}{2k_t} \mathrm{d}\overline{\lambda} = G_c \Delta \tag{3.8}$$

Where

$$\overline{\tau}_{max}(\overline{\lambda}) = \overline{\tau}(\xi = \overline{\lambda})$$

From Equation 3.7, it derives:

$$\overline{F}^2_{c,e}(\delta) = \frac{\delta}{\int_{\lambda-\delta}^{\lambda} \left(\frac{\rho + \cosh\left(\overline{\lambda}\right)}{\sinh\left(\overline{\lambda}\right)} \right)^2 \mathrm{d}\overline{\lambda}} \tag{3.9}$$

- **Shear criterion (Average formulation)**

  From what introduced in Chapter 2, it can be stated that in this specific case:

$$l_{ch} \int_{\lambda-\delta}^{\lambda} \tau_c \, \overline{\tau}(\xi) \, \mathrm{d}\xi = \tau_c \Delta \tag{3.10}$$

  and, again by using Equation 3.7, we obtain the $\overline{F}_{c,s}$:

$$\overline{F}_{c,s,a}(\delta) = \frac{\delta}{\sqrt{\mu} \int_{\lambda-\delta}^{\lambda} \frac{\rho \, \cosh(\lambda - \xi) + \cosh(\xi)}{\sinh(\lambda)} \mathrm{d}\xi} \tag{3.11}$$

- **Shear criterion (Leguillon's formulation)**

  By applying this latter formulation of the shear criterion it has been imposed that:

$$\overline{\tau}(\xi) \geq 1 \quad \text{for } \forall \xi \in (\lambda - \delta, \lambda) \tag{3.12}$$

  Considering the shape of the $\overline{\tau}$ the critical load is:

$$\overline{F}_{c,s,L}(\delta) = \frac{\sinh(\lambda)}{\sqrt{\mu} \, (\, \rho \, \cosh(\delta) + \cosh(\lambda - \delta) \,)} \text{ for } \forall \delta \in (0, \lambda - \xi_*) \tag{3.13a}$$

$$\overline{F}_{c,s,L}(\delta) = \frac{\sinh(\lambda)}{\sqrt{\mu} \, (\, \rho \, \cosh(\lambda - \xi_*) + \cosh(\xi_*) \,)} \text{ for } \forall \delta \in (\lambda - \xi_*, \lambda) \tag{3.13b}$$

  Where ξ_* is given by:

$$\overline{\tau}(\xi_*) = \min_{\xi \in (0,\lambda)} \overline{\tau}(\xi)$$

- **FFM model**

  According to what is illustrated in Equation 2.18, in this specific case the function of critical load given from the energy criterion $\overline{F}_{c,e}(\delta)$ is decreasing in its domain, while both $\overline{F}_{c,s,a}(\delta)$ and $\overline{F}_{c,s,L}(\delta)$ are increasing. The critical load is then found as the intersection of the curves given by the energy criterion and one of the shear criterion at the variation of δ. Figure 3.5 illustrates the situation for a given overlap length, the blue dot represents where the failure load is found and for which δ.

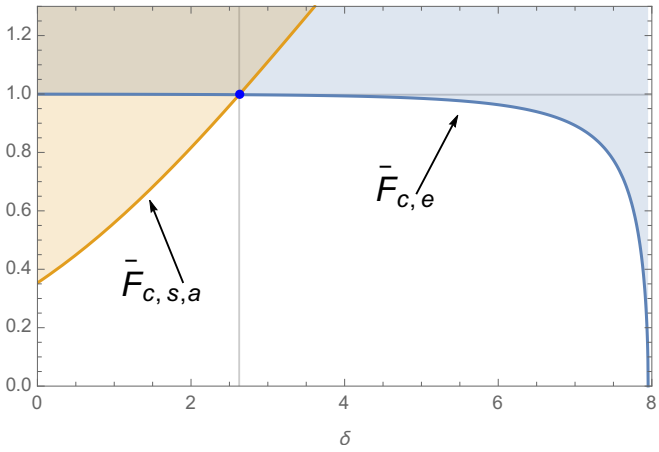

Figure 3.5: Plot of $\overline{F}_{c,s,a}(\delta)$ and $\overline{F}_{c,e}(\delta)$ for $\rho = 0.7$, $\mu = 8$ and $\lambda = 8$

Crack propagation on both sides

Figure 3.4 shows a quarter of the geometry of the double lap joint in case we consider finite crack propagation at both sides of two different lengths: Δ_r and Δ_l defined as in the figure.

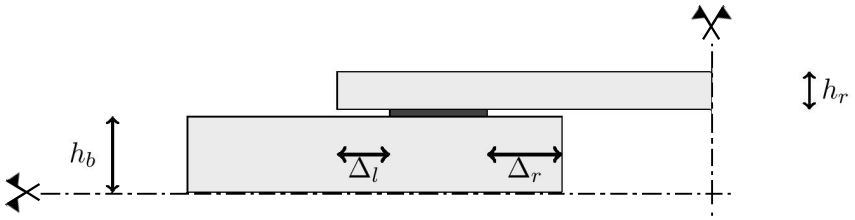

Figure 3.6: Crack propagation on the both sides

In this case we introduce the following dimensionless quantities:

$$\delta_r = \frac{\Delta_r}{l_{ch}}$$

$$\delta_l = \frac{\Delta_l}{l_{ch}}$$

- **Energy criterion**

In this specific case applying the energy criterion means:

$$l_{ch}\int_{\lambda-\delta_r}^{\lambda}\frac{\tau_{max,r}^2(\overline{\lambda})}{2k_t}\mathrm{d}\overline{\lambda}+l_{ch}\int_{\lambda-\delta_r-\delta_l}^{\lambda-\delta_r}\frac{\tau_{max,l}^2(\overline{\lambda})}{2k_t}\mathrm{d}\overline{\lambda}=G_c(\Delta_r+\Delta_l) \tag{3.14}$$

Where

$$\overline{\tau}_{max,r}(\overline{\lambda})=\overline{\tau}(\xi=\overline{\lambda})$$

and

$$\overline{\tau}_{max,l}(\overline{\lambda})=\overline{\tau}(\xi=0)$$

In Appendix A different ways for expressing this energy balance are illustrated. From Equation (3.7), it derives:

$$\overline{F}_{c,e}^2(\delta)=\frac{\delta_r+\delta_l}{\int_{\lambda-\delta_r}^{\lambda}\left(\frac{\rho+\cosh\left(\overline{\lambda}\right)}{\sinh\left(\overline{\lambda}\right)}\right)^2\mathrm{d}\overline{\lambda}+\int_{\lambda-\delta_r-\delta_l}^{\lambda-\delta_r}\left(\frac{1+\rho\ \cosh\left(\overline{\lambda}\right)}{\sinh\left(\overline{\lambda}\right)}\right)^2\mathrm{d}\overline{\lambda}} \tag{3.15}$$

- **Shear criterion (Average formulation, separated integrals)**

From what introduced in Chapter 2, it leads that in this specific case:

$$l_{ch}\int_{\lambda-\delta_r}^{\lambda}\overline{\tau}(\xi)\ \mathrm{d}\xi=\Delta_r \tag{3.16a}$$

$$l_{ch}\int_{0}^{\delta_l}\overline{\tau}(\xi)\ \mathrm{d}\xi=\Delta_l \tag{3.16b}$$

By using Equation 3.7, it is possible to obtain the explicit formulation of the $\overline{F}_{c,s,a}$ for each of the equation just illustrated, so we can call $\overline{F}^r_{c,s,a}$ the critical load obtained from the right side crack (Equation 3.16a), and $\overline{F}^l_{c,s,a}$ from the left side (Equation 3.16b), that can be expressed as:

$$\overline{F}^r_{c,s,a}=\frac{\delta_r}{\sqrt{\mu}\int_{\lambda-\delta_r}^{\lambda}\frac{\rho\ \cosh(\lambda-\xi)+\cosh(\xi)}{\sinh(\lambda)}\mathrm{d}\xi} \tag{3.17a}$$

$$\overline{F}^l_{c,s,a}=\frac{\delta_l}{\sqrt{\mu}\int_{0}^{\delta_l}\frac{\rho\ \cosh(\lambda-\xi)+\cosh(\xi)}{\sinh(\lambda)}\mathrm{d}\xi} \tag{3.17b}$$

- **Shear criterion (Average formulation, unique integral)**

Summing the equations (3.16a and 3.16b), it is possible to derive a unique $\overline{F}_{c,s,a}$ that has the following expression:

$$\overline{F}_{c,s,a}=\frac{\delta_r+\delta_l}{\sqrt{\mu}\left(\int_{\lambda-\delta_r}^{\lambda}\frac{\rho\ \cosh(\lambda-\xi)+\cosh(\xi)}{\sinh(\lambda)}\mathrm{d}\xi+\int_{0}^{\delta_l}\frac{\rho\ \cosh(\lambda-\xi)+\cosh(\xi)}{\sinh(\lambda)}\mathrm{d}\xi\right)} \tag{3.18}$$

While applying the coupled criterion, it is worth to note that from a mathematical point of view if $\overline{F}_c$ is satisfying the following constraint:

$$\overline{F}_c \geq \overline{F}_{c,s,a} \tag{3.19}$$

this does not imply that both:

$$\overline{F}_c \geq \overline{F}^r_{c,s,a} \tag{3.20a}$$

$$\overline{F}_c \geq \overline{F}^l_{c,s,a} \tag{3.20b}$$

are satisfied. This is the reason why both formulations have been used for the shear criterion, but, as it will be showed in the results, the differences in the critical load obtained with the FFM approach are really low.

- **Shear criterion (Leguillon's formulation)**

By applying this other formulation of the shear criterion it is obtained that:

$$\overline{\tau}(\xi) \geq 1 \quad \text{for } \forall \xi \in (\lambda - \delta_r, \lambda) \tag{3.21a}$$

$$\overline{\tau}(\xi) \geq 1 \quad \text{for } \forall \xi \in (0, \delta_l) \tag{3.21b}$$

Considering the shape of the $\overline{\tau}$ the critical load it's given by:
for the left side

$$\overline{F}^l_{c,s,L}(\delta_l) = \frac{\sinh(\lambda)}{\sqrt{\mu}\ (\ \rho\ \cosh(\lambda - \delta_l) + \cosh(\delta_l)\ )} \text{ for } \forall \delta_l \in (0, \lambda - \xi_{*,l}) \tag{3.22a}$$

$$\overline{F}^l_{c,s,L}(\delta_l) = \frac{\sinh(\lambda)}{\sqrt{\mu}\ (\ \rho\ \cosh(\lambda - \xi_{*,l}) + \cosh(\xi_{*,l})\ )} \text{ for } \forall \delta \in (\lambda - \xi_{*,l}, \lambda) \tag{3.22b}$$

for the right side

$$\overline{F}^r_{c,s,L}(\delta_r) = \frac{\sinh(\lambda)}{\sqrt{\mu}\ (\ \rho\ \cosh(\delta_r) + \cosh(\lambda - \delta_r)\ )} \text{ for } \forall \delta_r \in (0, \lambda - \xi_{*,r}) \tag{3.23a}$$

$$\overline{F}^r_{c,s,L}(\delta_r) = \frac{\sinh(\lambda)}{\sqrt{\mu}\ (\ \rho\ \cosh(\xi_{*,r}) + \cosh(\lambda - \xi_{*,r})\ )} \text{ for } \forall \delta \in (\lambda - \xi_{*,r}, \lambda) \tag{3.23b}$$

Where ξ_* is given by:

$$\overline{\tau}(\xi_{*,l}) = \overline{\tau}(\xi_{*,r}) = \min_{\xi \in (0,\lambda)} \overline{\tau}(\xi)$$

- **FFM model**
  For the case of double crack propagation, if for example we consider the separated integrals for the shear criterion, the critical load has to be grater or equal than $\overline{F}^l_{c,s,a}$, $\overline{F}^l_{c,s,a}$ and finally $\overline{F}_{c,e}$. A typical situation is represented in Figure 3.7. The dot is the intersection on the three lines that are plotted at the variation of the sum $\delta = \delta_r + \delta_l$ from 0 up to λ. The following plot represents where the minimum critical load is

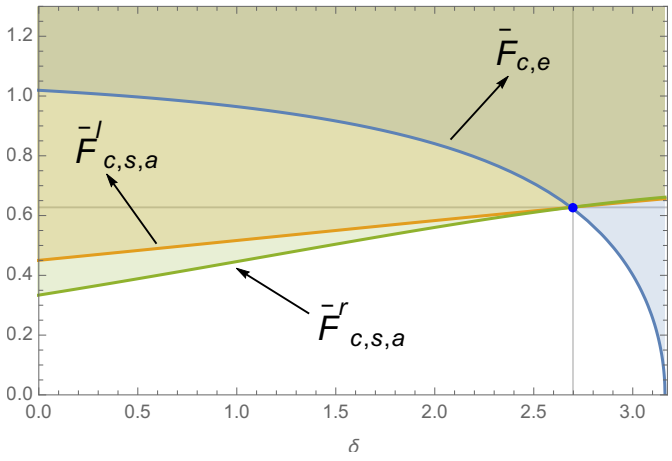

Figure 3.7: Plot of $\overline{F}^{l}_{c,s,a}(\delta)$, $\overline{F}^{r}_{c,s,a}(\delta)$ and $\overline{F}_{c,e}(\delta)$ for $\rho = 0.7$, $\mu = 8$ and $\lambda = 3.2$

found in case cracks are propagating on both sides. Note that, in case the crack is propagating on just one side, for example the right one, the curve of $\overline{F}^{l}_{c,s,a}$won´t be considered. Figure 3.8 is showing this specific case: even though the $\overline{F}^{l}_{c,s,a}$ is zero (because if there is no crack on that side the load needed for no crack to propagate is of course null), the critical load is found as the intersection of the other two curves. Again, the curves of the critical load from the shear criterion are all increasing

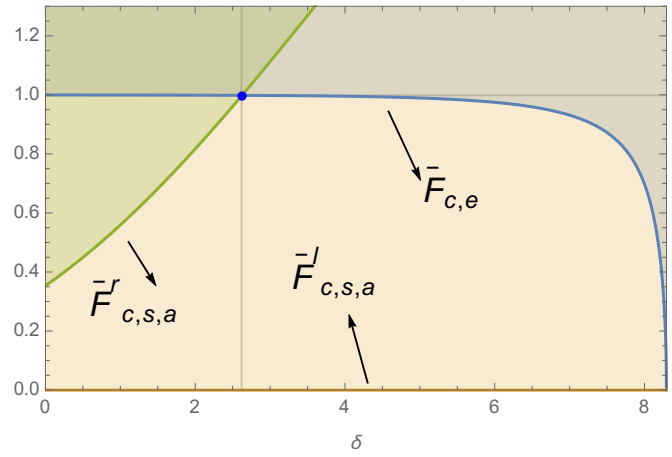

Figure 3.8: Plot of $\overline{F}^{l}_{c,s,a}(\delta)$, $\overline{F}^{r}_{c,s,a}(\delta)$ and $\overline{F}_{c,e}(\delta)$ for $\rho = 0.7$, $\mu = 8$ and $\lambda = 8.15$

for the methods just illustrated above, and the critical load given by the energy criterion is decreasing at the increasing of the sum δ, so the load is always found in correspondence of the intersection. The colored area of the parametric figures just mentioned indicates were a criterion is over full filled, in other words, the crack is

propagating for each loads that are in the area with the over positioning of all the colours.

Chapter 4

Single Lap Joint

In the following chapter the single lap joint configuration will be investigated with the tools illustrated in Chapter 2. Only the balanced configuration will be analyzed. Firstly, the study of the interface stresses is presented with two different methods: one considering only shear stress at the interface and one considering both shear and peel stresses; then the critical load will be investigated with the coupled criterion.

4.1 Description of the model

The Figure 4.1 shows the geometrical parameters that are describing the joint. The index a indicates the adhesive, the width of the geometry is defined by the quantity t. The parts to be joined have the modulus of elasticity E and the Poisson's number ν. The modulus of elasticity and shear of the adhesive layer and its Poisson's number are E_a, G_a and ν_a. The coordinate system lies in the middle of the adhesive layer.

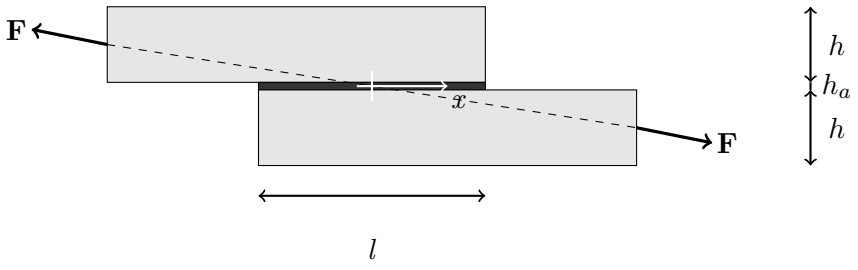

Figure 4.1: Single Lap Joint geometry

The assumption that the heights of the two block are the same is due to the difficulty that is encountered in case these are not equal. In fact, if this assumption is not done, the study of the stresses at the interface requires numerical computations because the stresses at the interface cannot be expressed explicitly depending on the other parameters. This

fact increases significantly the computational effort for the evaluation of the solution of the optimization problem presented before in Equation 2.19.
A quick illustration of two classical stress solutions at the interface is now presented. As as been done for the double lap joint, firstly we will present the solution obtained by considering only shear stresses at the interface and secondly the Goland-Reissner [8] model that takes into account both shear and peel stresses.

4.2 Shear lag model

4.2.1 Derivation of the interface stress

In the present model, the joining parts are modeled as rigid rods so the effect of bending deformations is excluded. For the adhesive layer, a linear-elastic relationship between the shear stress and the relative horizontal displacement is assumed, so it can be written that:

$$\tau = k_t s \tag{4.1}$$

Where k_t, the tangential stiffness, is given by:

$$k_t = \frac{G_a}{h_a}$$

and by indicating with the index 1 the upper block and 2 the lower one and with u the displacement in the direction perpendicular to the x-axis, s is defined as:

$$s = u_1 - u_2$$

Following a procedure similar to the one proposed for the double lap joint, it is possible to obtain the following differential equation, that derives from the applying constitutive and kinematic equations:

$$\frac{d^2 s}{dx^2} - \frac{2k_t}{Eh} s = 0 \tag{4.2}$$

by calling:

$$l_{ch} = \sqrt{\frac{Eh}{2k_t}}$$

the shear stress can be expressed in the following way:

$$\tau(x) = \frac{F}{2l_{ch}} \frac{\cosh(x/l_{ch})}{\sinh(l/2l_{ch})} \tag{4.3}$$

Similarly to what has been seen for the double lap joint, also for this specific symmetric geometry of the single lap joint the shear stress is symmetric respect to the mid point of the overlap region. The Figure 4.6 shows its shape, compared to the one that is found with the more complex model proposed by Goland-Reissner that will be explained later.

4.2.2 Critical load

The coupled criteria is presented now by considering Equation 4.3 of the shear stress at the interface. Also in this case, two different cases are considered:

- the crack propagates only on the side ;
- the crack propagates on both side of the same crack length.

After a deep study has been performed on the double lap joint geometry by considering different methods for applying the shear criterion, the average shear criterion has been preferred for studying this other joint configuration.

Crack propagation only on one side

Calling Δ the crack length, the situation is the one showed in the figure 4.2:

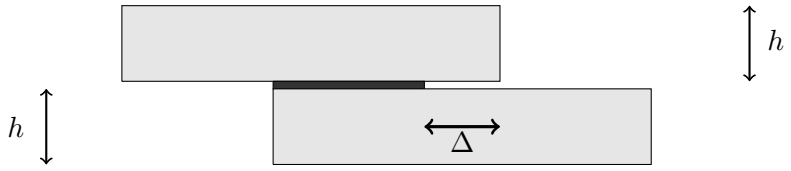

Figure 4.2: Crack propagation only on one side

- **Energy criterion** By the energy criterion , it leads that:

$$\Delta\Phi = \int_{l-\Delta}^{l} \frac{\tau_{max}^2(\bar{l})}{2k_t} \mathrm{d}\bar{l} = G_c\Delta \tag{4.4}$$

  Where

$$\tau_{max}(\bar{l}) = \tau(x = \bar{l}/2) = \tau(x = -\bar{l}/2).$$

  From which it can be explicitly derived the expression of the load $F_{c,e}(\Delta)$.

- **Shear criterion (Average formulation)** From what introduced in Chapter 2, it leads that in this specific case:

$$\int_{l/2-\Delta}^{l/2} \tau(x)\ \mathrm{d}x = \tau_c\Delta \tag{4.5}$$

  and, again by using Equation 4.3, it is possible to derive the expression of the critical load $F_{c,s,a}(\Delta)$.

- **FFM model**
  By using the coupled criterion, it is possible to derive the critical load. In this case it has to be noted that the shape of the $F_{c,s,a}$ at the variation of Δ for a fixed overlap

length is not always increasing. There are in fact some overlap lengths for which the situation is like the one showed in the figure 4.3. The following adimensionalization has been done in this case: Characteristic length: $l_{ch} = \sqrt{\frac{Eh}{2k_t}}$

Interface brittleness index: $\mu = \frac{2k_t G_c}{\tau_c^2}$

And:

$$\xi = \frac{x}{l_{ch}} \quad \lambda = \frac{l}{l_{ch}} \quad \delta = \frac{\Delta}{l_{ch}} \quad \overline{\tau} = \frac{\tau}{\tau_c} \quad \overline{F} = \frac{F}{F_c^{\infty}}$$

Where the F_c^{∞} is the failure load for infinite overlap length:

$$F_c^{\infty} = 2\sqrt{EhG_c} \tag{4.6}$$

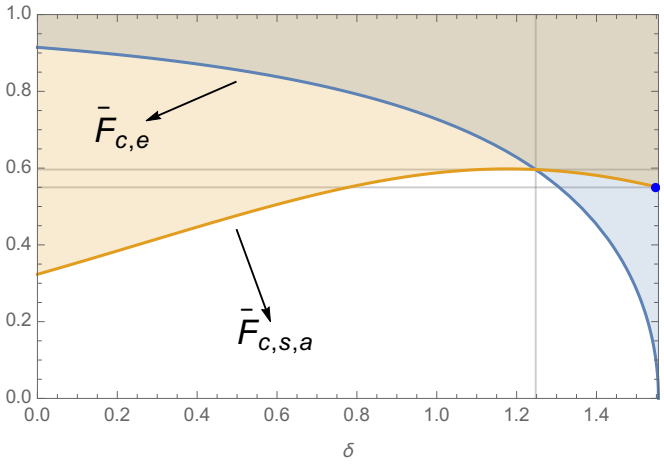

Figure 4.3: Plot of $\overline{F}_{c,s,a}(\delta)$ and $\overline{F}_{c,e}(\delta)$ for $\mu = 8$ and $\lambda = 1.55$

This is important for noticing that not always the coupled criterion implies that the minimum is found when both criterion are fulfilled but that it can be that minimum load is found where the shear criterion is over fulfilled.

Crack propagation on both sides

Considering the symmetry of the geometry and of the shear stresses in the overlap region it is possible to suppose that the crack propagates on both side of the same length Δ as showed in the figure 4.2

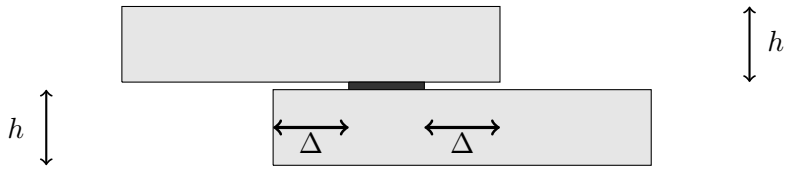

Figure 4.4: Crack propagation on both sides

- **Energy criterion**
  By the energy criterion , it leads that:

$$\Delta\Phi = \int_{l-2\Delta}^{l} \frac{\tau_{max}^2(\bar{l})}{2k_t} \mathrm{d}\bar{l} = 2G_c\Delta \tag{4.7}$$

  Where:

$$\tau_{max}(\bar{l}) = \tau(x = \bar{l}/2) = \tau(x = -\bar{l}/2).$$

  From which it can be explicitly derived the expression of the load $F_{c,e}(\Delta)$.

- **Shear criterion (Average formulation)**
  From what introduced in Chapter 2, it leads that in this specific case:

$$\int_{l/2-\Delta}^{l/2} \tau(x)\ \mathrm{d}x + \int_{l/2-\Delta}^{-l/2} \tau(x)\ \mathrm{d}x = \tau_c 2\Delta \tag{4.8}$$

  and, again by using Equation 4.3, it is possible to derive the expression of the critical load $F_{c,s,a}(\Delta)$.

- **FFM model**
  The critical load is then found by considering the two expression of $F_{c,e}$ and $F_{c,s,a}$ just mentioned and Equation 2.18 from Chapter 2. In this specific case, the critical load that derives from the shear criterion is increasing at the increasing of the Δ, so the critical load is found always at the intersection of the two curves. Basically the situation is similar to the one illustrated in the Figure 3.5.

With this basic model for the interface stresses in the single lap joint the solution of the coupled criterion is very simple due to the linearity of the load into the expression of the shear stress. In the model presented in the following section this cannot be performed anymore.

4.3 Goland-Reissner Model

4.3.1 Derivation of the interface stresses

The model of Goland and Reissner (1944) takes into account the bending deformation of the parts to be joined. In addition to shear stresses in the adhesive layer, peel stresses are

predicted. For the model only the overlap central region has been considered but, due to the bending deformation the cutting moment M_0 and the lateral force Q_0 at the extremes are non-linearly linked to the attacking force F due to the large bending deformations of the joining parts. For this purpose, a so-called moment factor k is introduced: it depends also on the force F. The determination of the correct nonlinear formulation has been the subject of many investigations. As shown the solution depends on the overlap length l, the joint thickness h and its width t. This definition is used in this work:

$$M_0 = kF\frac{h}{2} \tag{4.9a}$$

$$Q_0 = k'F \tag{4.9b}$$

where:

$$k = \frac{1}{2\sqrt{2}\tanh\left(\frac{l\sqrt{\frac{3}{2}(1-\nu^2)}\sqrt{\frac{F}{h_a \mathrm{E} h}}}{2h}\right) + 1} \tag{4.10a}$$

$$k' = \frac{h(1-k)+h_a}{l} \tag{4.10b}$$

this is the definition of the lateral force in the sense of Chen et al. Cheng (1983) [3] proposed as an improvement of the Goland-Reissner model. M_0 and T_0 are respectively the bending moment and the axial tension in the adherents at the extremes of the overlap region.
Again in this model the adhesive layer is considered as a bed of spring, so the following relation can be written:

$$\tau = G_a\frac{u_1 - u_2}{h_a} \tag{4.11a}$$

$$\sigma = E_a\frac{w_1 - w_2}{h_a} \tag{4.11b}$$

where u and w are respectively the displacements perpendicular and tangential to the x-axis and the index 1 indicate the upper block and 2 the lower one (referring to the figure 4.1). Again the tangential and the normal stiffness are defined by:

$$k_t = \frac{G_a}{h_a} \tag{4.12a}$$

$$k_n = \frac{E_a}{h_a}. \tag{4.12b}$$

According to the notation introduced, the differential equations describing the stresses that can be found in the work from Goland and Reissner [8], can be written in the following

way:

$$\frac{d^3\tau}{dx^3} - \frac{8G_a}{Ehh_a}\frac{d\tau}{dx} = 0 \tag{4.13a}$$

$$\frac{d^4\sigma}{dx^4} + \frac{24(1-\nu^2)E_a}{Eh^3h_a}\sigma = 0 \tag{4.13b}$$

That, by considering the initial conditions, depends also on the quantities M_0 and Q_0. The solution searched can be written like:

$$\tau(x) = \frac{F}{bL}\left(\frac{(1+3k)}{4}\frac{l}{2l_\tau}\frac{\cosh\left(\frac{x}{l_\tau}\right)}{\sinh\left(\frac{l}{2l_\tau}\right)} + 1 - \frac{(1+3k)}{4}\right) \tag{4.14}$$

where

$$l_\tau = \sqrt{\frac{Ehh_a}{8G_a}} \tag{4.15}$$

and

$$\begin{aligned}\sigma(x) =& F\frac{h}{\Gamma l_\sigma t}\left(\left(\frac{1}{2}k\ \frac{R_1}{l_\sigma} + \frac{2}{l}k'\ \sinh\left(\frac{l}{2l_\sigma}\right)\sin\left(\frac{l}{2l_\sigma}\right)\right)\sinh\left(\frac{x}{l_\sigma}\right)\sin\left(\frac{x}{l_\sigma}\right)\right) + \\ &+ F\frac{h}{\Gamma l_\sigma t}\left(\left(\frac{1}{2}k\ \frac{R_2}{l_\sigma} + \frac{2}{l}k'\ \cosh\left(\frac{l}{2l_\sigma}\right)\cos\left(\frac{l}{2l_\sigma}\right)\right)\cosh\left(\frac{x}{l_\sigma}\right)\cos\left(\frac{x}{l_\sigma}\right)\right)\end{aligned} \tag{4.16}$$

with:

$$l_\sigma = \sqrt[4]{\frac{Eh^3h_a}{6E_a(1-\nu^2)}} \tag{4.17a}$$

$$\Gamma = \frac{1}{2}\left(\sinh\left(\frac{l}{l_\sigma}\right) + \sin\left(\frac{l}{l_\sigma}\right)\right) \tag{4.17b}$$

$$R_1 = \cosh\left(\frac{l}{2l_\sigma}\right)\sin\left(\frac{l}{2l_\sigma}\right) + \sinh\left(\frac{l}{2l_\sigma}\right)\cos\left(\frac{l}{2l_\sigma}\right) \tag{4.17c}$$

$$R_2 = \sinh\left(\frac{l}{2l_\sigma}\right)\cos\left(\frac{l}{2l_\sigma}\right) - \cosh\left(\frac{l}{2l_\sigma}\right)\sin\left(\frac{l}{2l_\sigma}\right) \tag{4.17d}$$

The typical shape of those stresses is showed in the figure 4.5. Differently from the double lap joint, the peeling is not going down to zero quickly in the zone more far away from the edges so it is significant to take it into account. The plot has been done by using the material proprieties of the experiment from Da Silva et al. [7] (the material values are in Table 5.2), for a load applied $F = 8000N$ and a total overlap length of: $l = 9mm$. As already mentioned before, the difference between this model and the one that does not take into account the peeling stresses is significant. In the results this difference will be showed also in terms of critical load. For the same geometry of the Figure 4.5, the Figure 4.6 shows the differences between the two different shear stresses from the two models proposed above. Both plots are symmetric as expected but, of course, if the peeling is not considered the value of the shear stress at the edges is higher than the one from the Goland-Reissner model.

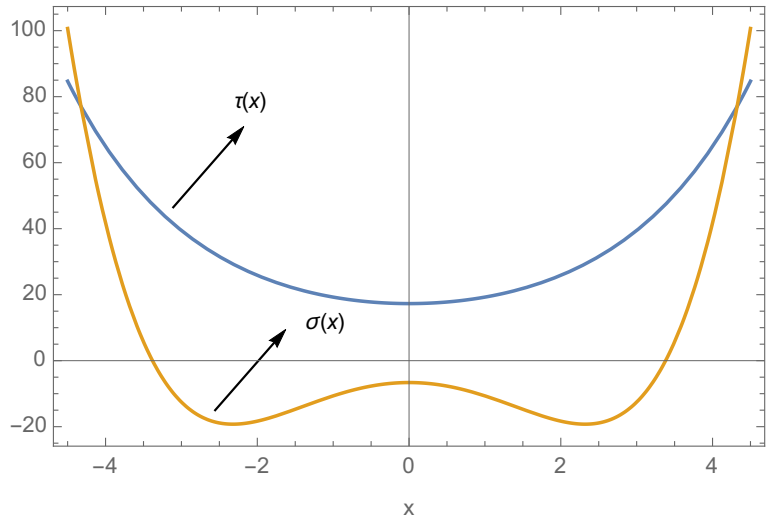

Figure 4.5: Plot of $\tau(x)$ and $\sigma(x)$ for $F = 8000N$, $l = 9mm$ and the material parameters found in the

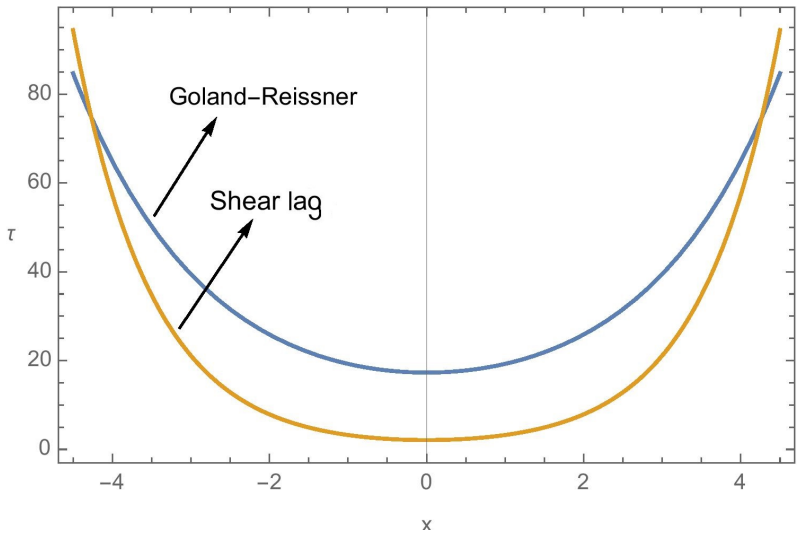

Figure 4.6: Comparison between the $\tau(x)$ from the shear lag and the Goland-Reissner models. $F = 8000N$, $l = 9mm$ and the material parameters of 5.2 (Redux 326)

4.3.2 Critical load

The coupled criteria will be now presented considering the solution for the stresses at the interface that have been just found. In this case the mixed mode fracture has been considered. Also in this case, two different cases are taken into account:

- The crack propagates only on the side ;
- the crack propagates on both side of the same crack length.

The average stress criterion as been preferred for this specific case. Due to the impossibility to explicitly write the critical load in function of the crack length (as it can be done for all the other cases illustrated in this work) the critical load is found by numerically solving a minimization problem subjects to the constraints given by the coupled criterion depending on both the critical load and the crack length interpreted as variables.

Crack propagation only on one side

Referring to the situation of figure 4.2, the crack length will be called Δ.

- **Energy criterion**
  Applying the energy criterion in this case means that the following inequality has to be considered:
  $$\frac{1}{\Delta}\int_{l-\Delta}^{l}\left(\frac{\tau_{max}^2(\bar{l})}{2k_t}+\frac{\sigma_{max}^2(\bar{l})}{2k_n}\right)\mathrm{d}\bar{l}\geq G_c \tag{4.18}$$
  Where
  $$\tau_{max}(\bar{l})=\tau(x=\bar{l}/2) \tag{4.19a}$$
  $$\sigma_{max}(\bar{l})=\sigma(x=\bar{l}/2) \tag{4.19b}$$

- **Stress criterion (average formulation)**
  As illustrated in Equation 2.15 for the mode mixity, the stress criterion can be written in the following way:
  $$\frac{1}{\Delta}\int_{l/2-\Delta}^{l/2}\left(\frac{\sigma(x)}{2}+\sqrt{\left(\frac{\sigma(x)}{2}\right)^2+\tau^2(x)}\right)\mathrm{d}x\geq\sigma_c \tag{4.20}$$
  That is, it is required the Rankine stress criterion to the fulfilled (on average) over the finite crack increment Δ.

- **FFM solution**

  Due to the impossibility to derive the explicit equation for the failure loads from the two criteria, it is not possible to perform a parametric plot of the $F_{c,e}(\Delta)$ and $F_{c,s}(\Delta)$. In order to solve the optimization problem (Equation 2.19), the solution is found by searching the minimum F that satisfy both the inequalities 4.18 and 4.20, and adding the constrain: $\Delta\in[0,l]$. With a posteriori analysis it has been checked that the minimum is always found where both expression are actually strictly satisfied, this implies that an hypothetical parametric plot of $F_{c,e}(\Delta)$ and $F_{c,s}(\Delta)$ would have found the minimum in the intersection. In Section 5.2 more detail about how the solution has been found with the used software will be shown.

Crack propagation on both sides

Referring to the situation of figure 4.4, the crack lengths will be called Δ and they are supposed to have the same length on both sides.

- **Energy criterion**
  The energy criterion leads the following inequality:

$$\frac{1}{2\Delta}\left(\int_{l-2\Delta}^{l}\left(\frac{\tau_{max}^2(\bar{l})}{2k_t}+\frac{\sigma_{max}^2(\bar{l})}{2k_n}\right)\mathrm{d}\bar{l}\right)\geq G_c \tag{4.21}$$

  Where

$$\tau_{max}(\bar{l})=\tau(x=\bar{l}/2)=\tau(x=-\bar{l}/2) \tag{4.22a}$$
$$\sigma_{max}(\bar{l})=\sigma(x=\bar{l}/2)=\sigma(x=-\bar{l}/2) \tag{4.22b}$$

- **Stress criterion (average formulation)**
  As illustrated in Equation 2.19 for the mode mixity, the shear criterion, supposing that the fracture propagates from both sides of the overlap region, can be written in the following way:

$$\frac{1}{2\Delta}\Big(\int_{l/2-\Delta}^{l/2}\left(\frac{\sigma(x)}{2}+\sqrt{\left(\frac{\sigma(x)}{2}\right)^2+\tau^2(x)}\right)\mathrm{d}x+ \int_{-l/2}^{-l/2+\Delta}\left(\frac{\sigma(x)}{2}+\sqrt{\left(\frac{\sigma(x)}{2}\right)^2+\tau^2(x)}\right)\mathrm{d}x\Big)\geq\sigma_c$$

- **FFM solution**
  The solution for this specific case has been found by using the same illustrated in the above case of propagation only on one side. With the only difference that the Δ is allowed to be only for: $\Delta\in\left[0\ ,\ \frac{l}{2}\right]$. Obviously for higher values the total crack length (2Δ) would be grater than the overlap length, that is physically impossible.

Chapter 5

Results, analysis and discussion

In this chapter are presented the results of the methods illustrated in the previous chapters with parametric analysis, comparisons with experimental results and observations for both double and single lap joint configurations. Moreover, a comparison with LEFM, MSSC and CCM is showed. All the evaluation has been performed by using the software Mathematica (version 11).

5.1 Double lap joint

According to the notation introduced in Chapter 3, the first result that is showed is a parametric non-dimensional analysis of the critical load $\overline{F}_c$ vs. the overlap length λ. Figure 5.1 shows the typical shape of this curve. This results has been evaluated by using the shear lag method and considering crack propagation on both sides with the average (separated formulation) shear criterion. As it is possible to notice from the figure, for λ larger than a certain threshold, that we will call λ_{Eff}, the critical load tends to a flat region with a value close to 1, that means that $F \cong F_c^{\infty}$. In this specific illustration the value of λ_{Eff} refers to maximum critical load reached with an error of the 1 It also interesting to see how the crack lengths δ_r and δ_l vary along with λ. Figure 5.2 shows the two propagation for the same parameters of Figure 5.1. The graph shows that the crack propagates on both side only for some overlap lengths, but after a certain value of λ (that it has been called λ_{th}) is reached, there is propagation only on the right side of the adhesive. This is a typical situation for $\rho < 1$, where the shear stresses reach higher value at the right side of their domain (see Figure 3.3). A parametric study of the crack propagation lengths as ρ varies will be showed later with a deep study on when crack is propagating on both extremes. Note that, λ_{th} and λ_{Eff} are not coincident; moreover, the curve of $\overline{F}_c$ shows a slight change in the slope in the correspondence of $\lambda = \lambda_{th}$.
The study of the variation of the critical load and the crack lengths has been performed on all the multiple methods illustrated in Chapter 3 and, in the following section, it will be showed how these graphs are changing along with the used method.

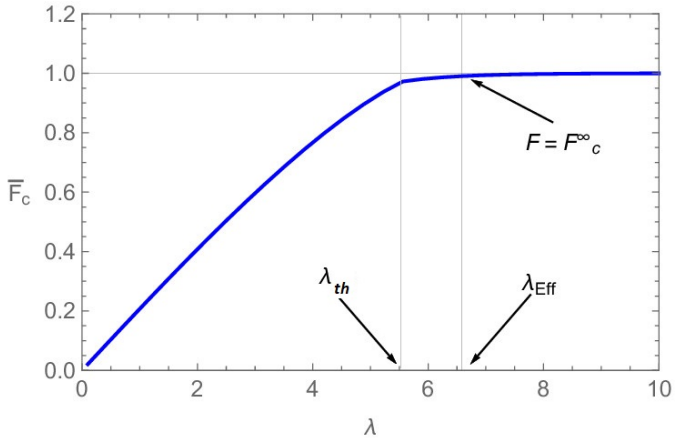

Figure 5.1: Plot of $\overline{F}_c(\lambda)$ for $\rho = 0.7$, $\mu = 8$

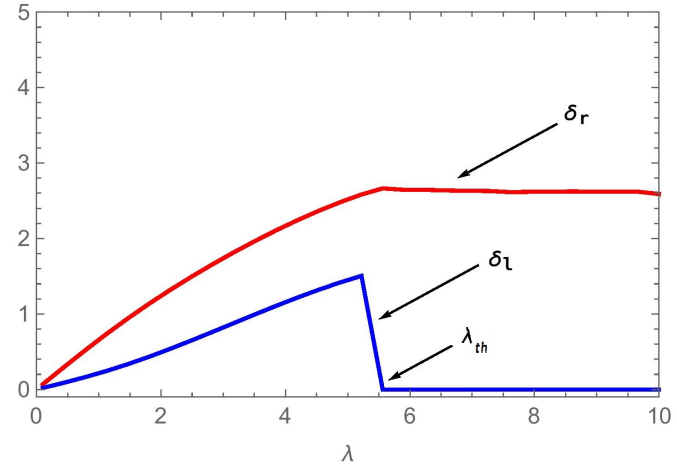

Figure 5.2: Plot of $\delta_r(\lambda)$ and $\delta_l(\lambda)$ for $\rho = 0.7$, $\mu = 8$

5.1.1 Comparison between average shear method and Leguillon's method

Crack propagation on both sides

The comparison of results between the average shear method and Leguillon's method is illustrated in the case of crack propagation on both side at the variation of the overlap length. Figure 5.3 shows the solution found with the average shear criterion (both unique and separated integrals) and the Leguillon's criterion. Some observations:

- as it can be easily predicted, the average criteria in correspondence of the same overlap length predict a lower value of the critical load;
- the critical load curves for the two average shear criteria are almost coincident;

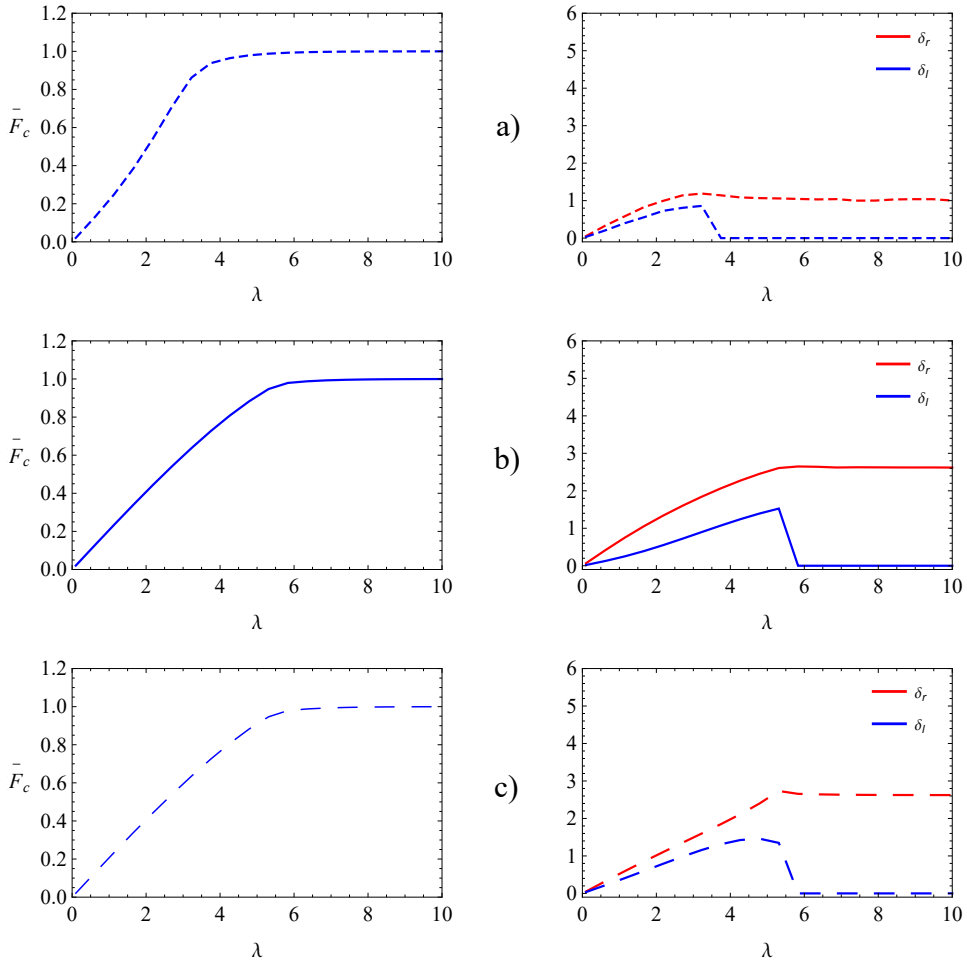

Figure 5.3: Plot of $\overline{F}_c(\lambda)$ (first column) and $\delta_r(\lambda)$ and $\delta_l(\lambda)$ (second column) for $\rho = 0.7$, $\mu = 8$. From the top to the button by using: a) Leguillon´s method, b) Average shear criterion separated integrals and c) Average shear criterion unique integral

- the L_{Eff} found with Leguillon method is always lower than the one predicted with the average criterion;
- the values of δ_r and δ_l given by using the average shear criterion are higher than the one from the Leguillon´s method due to the fact that the results given by the integral of the shear stress over the crack length as to be performed on a wider domain in order to obtain the desired τ_c;
- the shapes of the crack lengths of the two average shear criterion are mostly the same, but the one obtained by performing the unique integral is smoother;
- from a numerical point of view all the solutions are found by using the `FindMinimum`

function of the software Mathematica. In particular by writing the problem in the following way:

$$\begin{aligned} &\texttt{FindMinimum}\ F_{c,e}(\delta_r, \delta_l) \\ &\quad \texttt{subject to}\ F_{c,e}(\delta_r, \delta_l) \geq F^r_{c,s,*}(\delta_r, \delta_l) \\ &\qquad\qquad\quad F_{c,e}(\delta_r, \delta_l) \geq F^l_{c,s,*}(\delta_r, \delta_l) \\ &\qquad\qquad\quad \delta_r + \delta_l \in [0.0, \lambda] \end{aligned}$$

where the $*$ is indicating either a or L. Note that, every calculation has to be performed at a fixed value for λ. To obtain the curve of Figure 5.1 and Figure 5.3 the interval $\lambda \in [0.0,\ 10]$ has been discretizied in 50 points. The `FindMinimum` function is using the conjugate-gradient method: the solver is finding a local minimum, and this appeared to be also a global minimum only in case the average unique integral shear method was chosen, independently from the starting point that was given to the solver. For the other two methods a grill of points over the domain of $\delta_r + \delta_l \in [0.0, \lambda]$ as been defined, then the `FindMinimum` has to be evaluated from all those different starting points and by comparing the local minimum found for a fixed λ, the minimum between them gives the global one.

- the solution with the average unique integral took approximately 5 second on a normal personal computer. For the other two methods a starting grill of 99 points has been used and the solver took approximately 6 minutes for each of them.

Crack propagation on one side

The comparison between average shear method and Leguillon's method has also be performed under the hypothesis that the crack is propagating only on one side. By using the same assumptions of the problem solved in Figure 5.3, Figure 5.4 shows the solution given by this other method with the gray lines. The following observations can be done:

- the solution of this case is simpler: according to the fact that the critical load is found in the intersection of the two curves $F_{c,e}(\delta)$ and $F_{c,s,*}(\delta)$ (see Figure 3.5), the function

  $$\texttt{FindRoot}[F_{c,e}(\delta) = F_{c,s,*}(\delta),\ \delta \in [0,\ \lambda]]$$

  can be used for all the shear methods. The $*$ indicates either a or L. By using the same assumptions of the problem solved in Figure 5.3 the solver took approximately 3 seconds for every kind of shear method used.

- as it can be easily predicted the average criterion, for the same overlap length, predicts a lower value of the critical load (for one side crack propagation results);

- the critical load curves for the two average shear criteria are almost coincident;

- the L_{Eff} found with the same criterion but with considering propagation only on one side is lower that the one predicted with the double crack propagation;

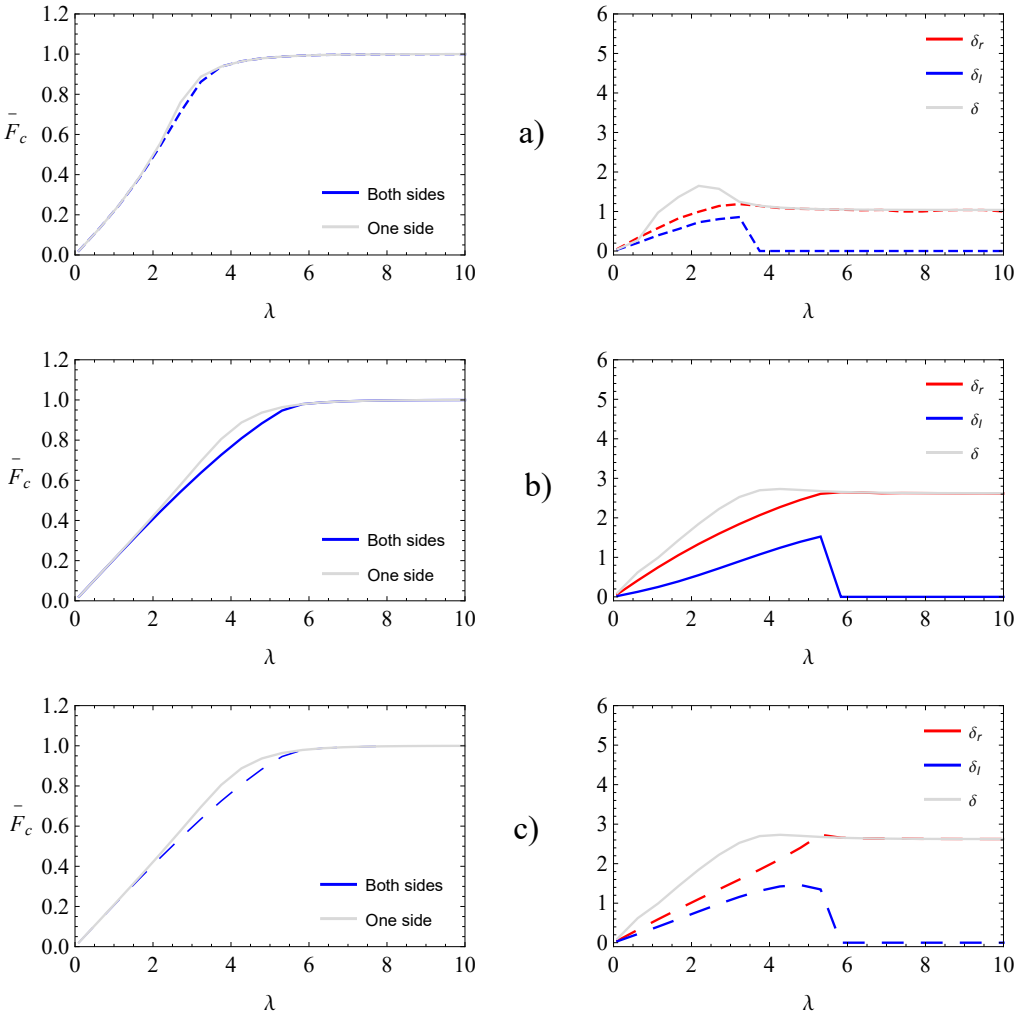

Figure 5.4: Plot of $\overline{F}_c(\lambda)$ (first column) by supposing both propagation on one and both sides and $\delta_r(\lambda)$ and $\delta_l(\lambda)$ (second column) for $\rho = 0.7$, $\mu = 8$. From the top to the button by using: a) Leguillon´s method, b) Average shear criterion separated integrals and c) Average shear criterion unique integral

- the values of δ_r and δ are coincident in the overlap region where δ_l is null;
- the shapes of the crack lengths of the two average shear criterion (of one side crack propagation results) are approximately the same.

After having analyzed the different shear criteria that can be used, the average criterion with the unique integral has been used for all the results that will be shown below according to the fact that is the faster one and gives a good prediction of the critical load. The fact that the load vs overlap length curves of the row b) and c) of Figure 5.3 are almost coincident also ensures that the inequalities of equations 3.20a and 3.20b hold true.

5.1.2 Comparison between propagation on one or both sides.

In the study of which of this two assumptions is predicting the minimum critical load, the ρ parameter is playing an important role. The model is in fact predicting that, for low values of ρ (that means strongly unbalanced joints) stress concentration is high only on one side of the geometry and the crack is actually only propagating on that side; while, for value of ρ close to 1 the crack is propagating on both and a lower critical load is given by the both sides propagation model. Figure 5.5 is showing the critical load obtained for a $\rho = 0.9$, $\mu = 8$ and $\lambda \in [0,10]$. The important thing that has to be noticed it that

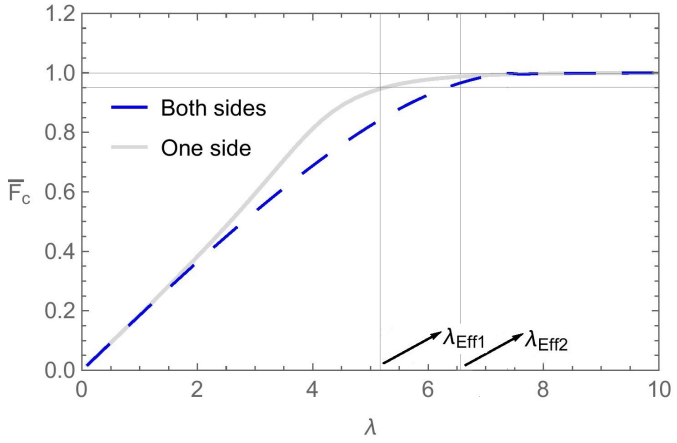

Figure 5.5: Plot of $\overline{F}_c(\lambda)$ by supposing both propagation on one and both sides for $\rho = 0.9$, $\mu = 8$.

the λ_{Eff1} (predicted from only one side propagation) and λ_{Eff2} (two sides) are different. $\lambda_{Eff1,2}$ refers to maximum critical load reached with an error of the 5%. Considering crack propagation on one side in a structure that has interface stresses that are almost symmetric compared to the mid-length of the interface actually yields a λ_{Eff} that is lower. This underestimation can be dangerous in designing DLJs.
For a deeper understanding of this difference Figure 5.6 shows the results for different values of ρ. Starting from the top row, it is possible to notice that this is a case where there is no need in supposing crack propagation on both sides, while the bottom row clearly shows how the crack is actually the same ($\delta_r = \delta_l$) if the geometry is symmetric (and also the stresses at the interface are symmetric). This is the reason why, as illustrated in Chapter 4, for a symmetric single lap joint the crack is supposed to propagate on both sides of the same length.
The model that has been preferred to achieve the remaining predictions is the one that supposes propagation on both sides. The reason is well defined: this model is able to predict (at the variation of the geometry) if the crack is actually starting on one or both edges.

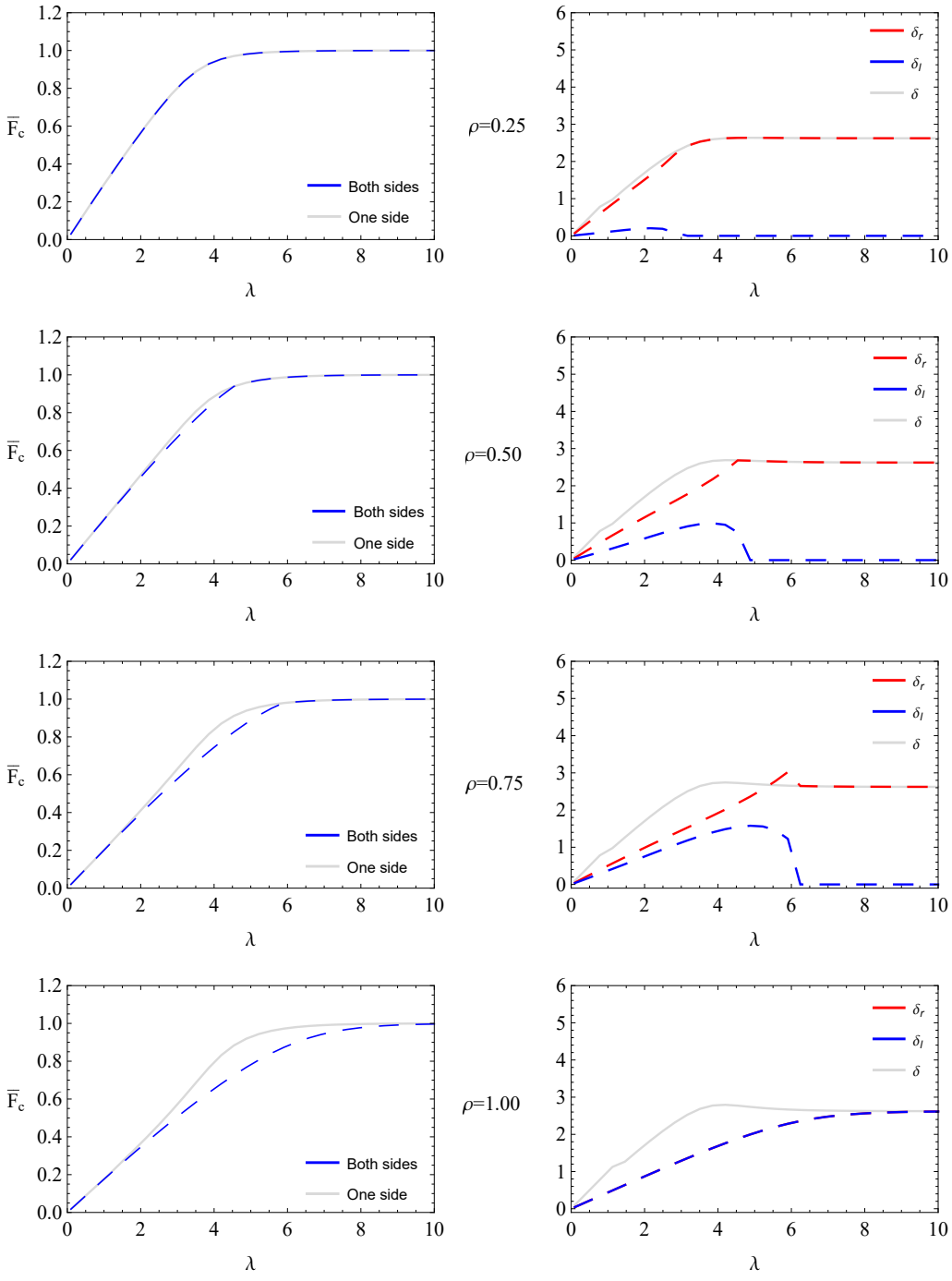

Figure 5.6: Plot of $\overline{F}_c(\lambda)$ and $\delta(\lambda)$, $\delta_l(\lambda)$ and $\delta_r(\lambda)$ by supposing propagation on one and both sides varying ρ ($\mu = 8$).

5.1.3 Parametric analysis

Mechanical fraction of the reinforcement

It is interesting to see the how the critical load vs. overlap length curves changes along with the mechanical fraction of the reinforcement:

$$\rho = \frac{E_r t_r h_r}{E_b t_b h_b}$$

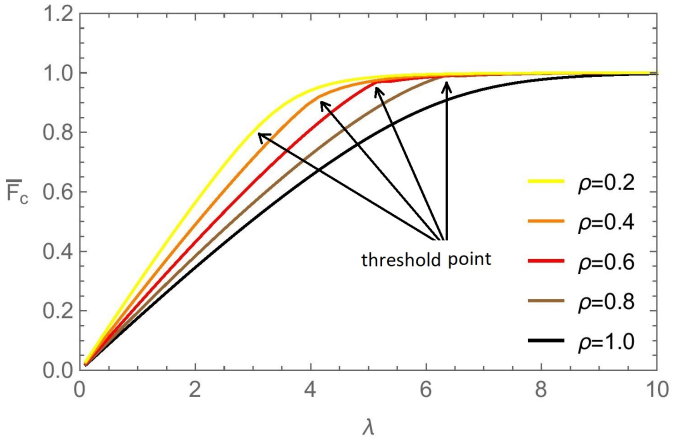

Figure 5.7: Plot of $\overline{F}_c(\lambda)$ at variation of ρ. ($\mu = 8$).

Figure 5.7 shows for $\mu = 8$ how the maximum bearing load is reached faster as the overlap length increases if the mechanical fraction reinforcement ρ is lower. This implies also that the higher is the ρ, the higher λ_{Eff}. According to the notation introduced in Chapter 3, here is considered only $\rho \in (0.0,1.0]$, but analogous results hold for $\rho > 1$.
What is also interesting to see is how the λ_{th} changes along with the ρ. As already presented before, there is a change in the shape in correspondence of $\lambda = \lambda_{th}$. Figure 5.7 shows where is the critical point: the change of the slope is sharper for high values of ρ.
This comparison has been performed by supposing crack propagation on both sides. If it would have been done under the other hypothesis, the difference between the different curves at the variation of ρ would not have been as clear as with this one presented.

Interface brittleness number

The physical meaning of the interface brittleness index μ has been introduced in Chapter 3. For the considered model it can be written as:

$$\mu = \frac{2k_t G_c}{\tau_c^2}$$

Figure 5.8 shows for $\rho = 0.7$ how this parameter is influencing the shape of the function $\overline{F}_c(\lambda)$. Note that $\mu = 1$ corresponds to a linear elastic-perfectly brittle interface behaviour

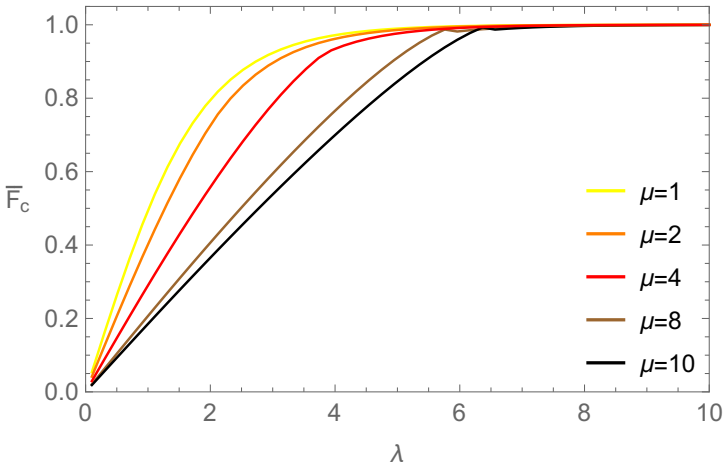

Figure 5.8: Plot of $\overline{F}_c(\lambda)$ at variation of μ ($\rho = 0.7$).

and $\mu \to \infty$ to a linear elastic perfectly plastic interface. In particular, the solution for $\mu = 1$ is the same as the LEFM solution. In fact the crack advancement provided by the application of the FFM model is infinitesimal and the energy condition for crack propagation coincides with the attainment of the peak strength at the crack tip ($\tau_{max} = \tau_c$). As expected, in the graph the values of the critical load tend more rapidly to the critical load close if μ is smaller. Moreover, this model predicts an increase of the λ_{Eff} as the ductility of the interface increases.

5.1.4 Comparison with other methods

The comparison with the LEFM, maximum shear stress criterion and the analytic solution with the cohesive crack model (CCM) provided by Biscaia & Chastre [1] is shown in this section.

Comparison with LEFM and maximum shear stress criterion

As it was already studied in the article *Finite fracture mechanics at elastic interfaces* [5], the finite fracture mechanic approach suggests that the prediction provided by LEFM should be considered more reliable than the one obtained with the maximum shear stress criterion (MSSC). This two methods have been introduced in Chapter 2. However, for interfaces with a high brittleness index, or a short overlap length, LEFM overestimates the failure load, as can be seen in Figure 5.9. Figure 5.10 is instead showing the comparison between these methods for $\mu = 2$. As already mentioned in the parametric analysis on the brittleness index, for a values of μ equal to 1, the FFM criterion reverts to LEFM criterion. In the case illustrated in Figure 5.10, the two curves from the just mentioned models are close by, and this result is in perfect agreement with what just presented.

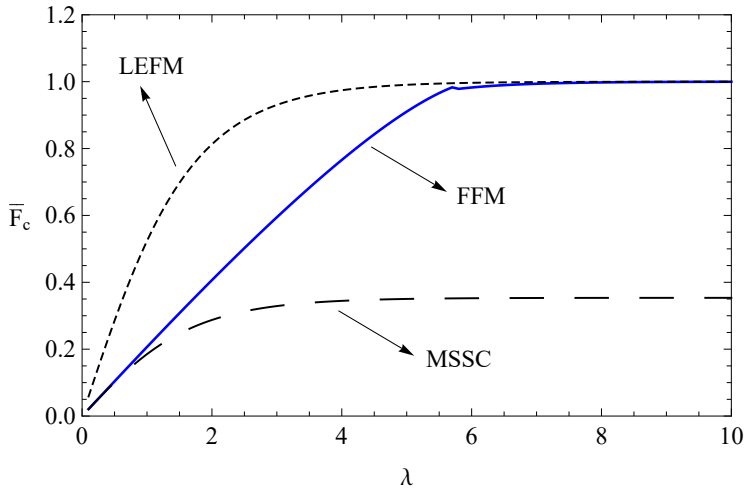

Figure 5.9: Plot of $\overline{F}_c(\lambda)$ for $\rho = 0.7$ and $\mu = 8$ with LEFM, FFM and MSSC.

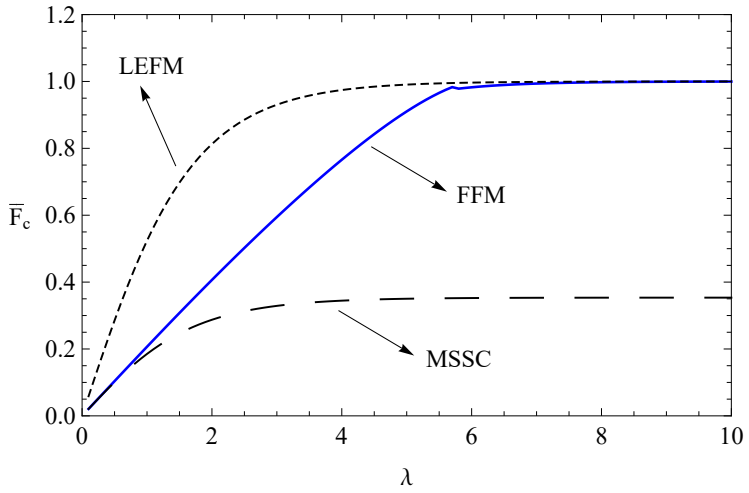

Figure 5.10: Plot of $\overline{F}_c(\lambda)$ for $\rho = 0.7$ and $\mu = 2$ with LEFM, FFM and MSSC.

Comparison with analytic solution with the cohesive crack model

Thanks to the work published by Biscaia & Chastre [1], it has been possible to compare the solution provided by the finite fracture mechanic approach to the one given by an analytic solution with the cohesive crack model. In this solution the peel stresses are disregarded as it has been done in this study. The results have been compared with the one of Figure 7 of the above cited article, where the failure load vs. overlap length is showed for different values of the mechanical fraction of the reinforcement ρ. In particular, the brittleness number of this specific geometry is equal to $\mu = 7.41$. All the other geometrical

proprieties can be found in the paper. The comparison is showed in Figure 5.11 where the

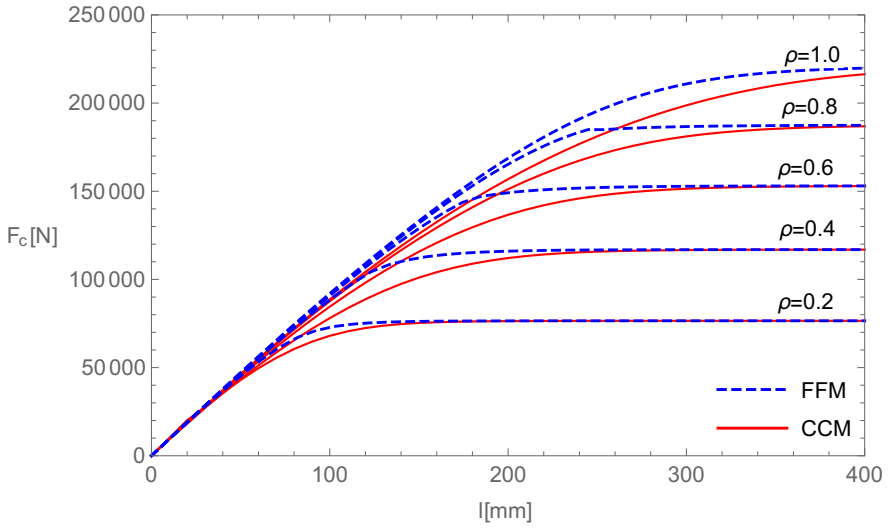

Figure 5.11: Plot of $F_c(l)$ of this solution and the one from [1] for different ρ. $\mu = 7.41429$

dashed blue line is the solution obtained by FFM (with the average criterion) and the red line is the results given by CCM (analytic solution by Biscaia & Chastre).

Another comparison has been done against the result obtained by considering a geometry with $\mu = 2$. Figure 5.12 shows the results for this specific case, where λ values have been discretized in 10 different values.

The results have been also compared to the one given by Leguillon´s formulation but the discrepancy was higher. In fact, Cornetti et al. presented an analytical comparison between FFM and CCM [6] and in their work it was shown that Leguillon´s (point-stress) formulation is in better agreement with a Dudgale shape for the cohesive law. According to the fact that the cohesive law used by Biscaia & Chastre [1] shows a linear softening, it was already expected that the average criterion fits better with the analytical results from the CCM.
The trend of the two solutions are very similar. For small bonded lengths the value are the same, but as the bonded length increases and the softening regime develops within the interface there are some discrepancies. The FFM approach gives λ_{Eff} that are slightly smaller than the ones from the CCM proposed here. Looking at the differences between the comparison with the two different μ, it can be notice that, if the brittleness index is smaller, the two trends are more similar especially for value of ρ at the extremes of the interval [0.0 , 1.0].

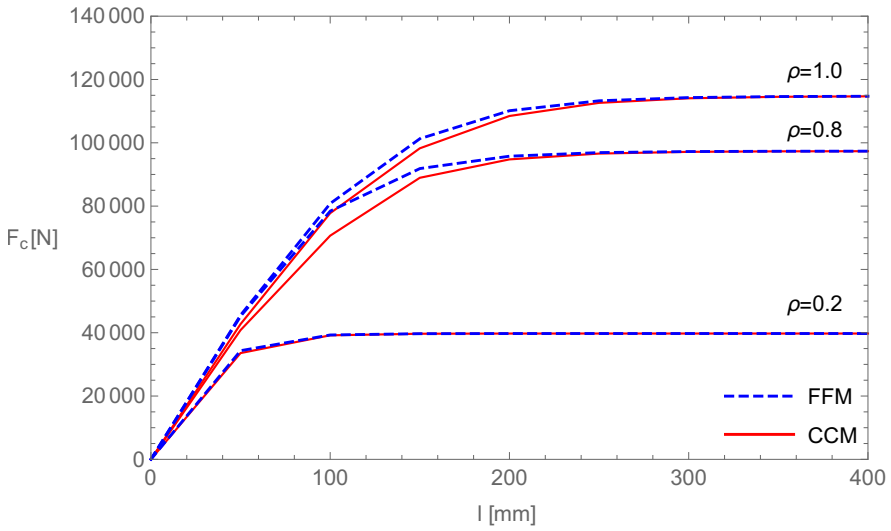

Figure 5.12: Plot of $F_c(l)$ of this solution and the one from [1] for different ρ. $\mu = 2$

5.1.5 Comparison with experimental results

Two comparisons with experimental data are now showed. Unfortunately, due to the difficulties of the tension test with double lap joint configuration experimental setup, the propagation of error on the results that can be found in literature is usually high. The material parameters for both experiment setup analyzed are in Table 5.1.

	E_a (N/mm^2)	h_r (mm)	h_b (mm)	h_a (mm)	$t_r = t_a$ (mm)	$E_r = E_b$ (MPa)
Mendoza-Navarro et al.[15]	3130	3.0	1.5	0.5	12.5	200
Campilho et al.[2]	4890	3.0	1.5	0.2	20	70

Table 5.1: Parameter from the two experimental setups from Mendoza-Navarro et al. [15] and Campilho et al. [2].

Comparison A

The model is applied to the geometry used in the "Type B" adhesive joint test from Mendoza-Navarro [15]. As has been done in the cited article, the parameters τ_c and G_c are determined by fitting the prediction to the experimental data test found in the article and applying a least square method. In this way, due to the fact that the experiment has been done just for three different overlap lengths (i.e. $l = 10mm$, $l = 15mm$, $l = 20mm$) the values τ_c and G_c obtained are not really reliable.
The results found are:

$$\tau_c = 10.3 \text{ MPa}$$

$$G_c = 0.0276 \text{ N/mm}$$

Figure 5.13 shows in orange the values found in Table 3 of the considered article [15], and with the gray line the FFM prediction with the τ_c and G_c just presented. The results are

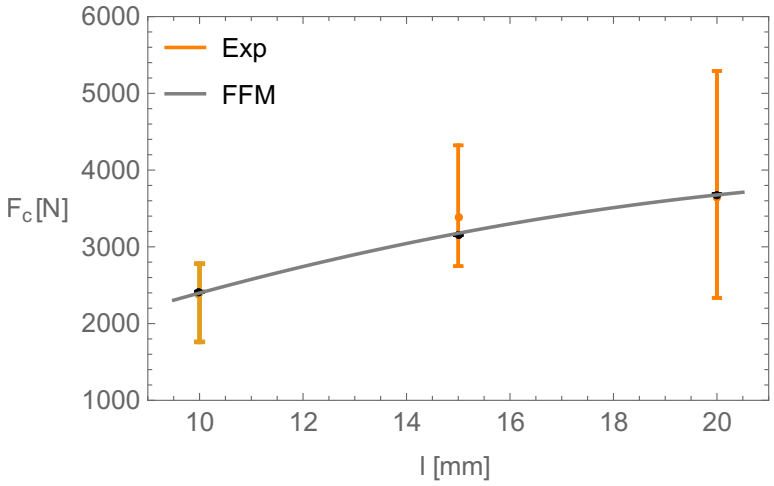

Figure 5.13: Comparison with the experimental result of the Type B test from [15]

perfectly fitting and, the finite fracture mechanic is predicting that in the case $l = 10mm$, there is propagation of the crack on both side while for longer value the crack is propagating on only one. It has to be noted that, with this experimental setup, the mechanical fraction of the reinforcement is $\rho = 2$; this implies that the model has to be adapted to this case and the crack length is predicted to be higher on the right side differently from what seen in the previous cases. Details can be found in the Appendix B. The lengths of the joint used in the experiment are extremely small so it was not really possible in this experimental setup to check if the crack is actually present at both edges of the adhesive. The main goal of this study was to predict the failure load.

Comparison B

A second comparison has been performed by using the experimental result from Campilho et al. [2]. Also for this case the parameters τ_c and G_c are determined by fitting the predictions to the experimental data test found in the article and applying a least square method. The results found are:

$$\tau_c = 20.2 \text{ MPa}$$

$$G_c = 0.218 \text{ N/mm}$$

They are different compared to the one used for the prediction of the article because the model used there for the fitting is different. The comparison of the results is showed in Figure 5.14; also for this geometry ρ was equal to 2. The model is predicting fairly well the values for this test; the failure load is increasing at the increase of the l parameter.

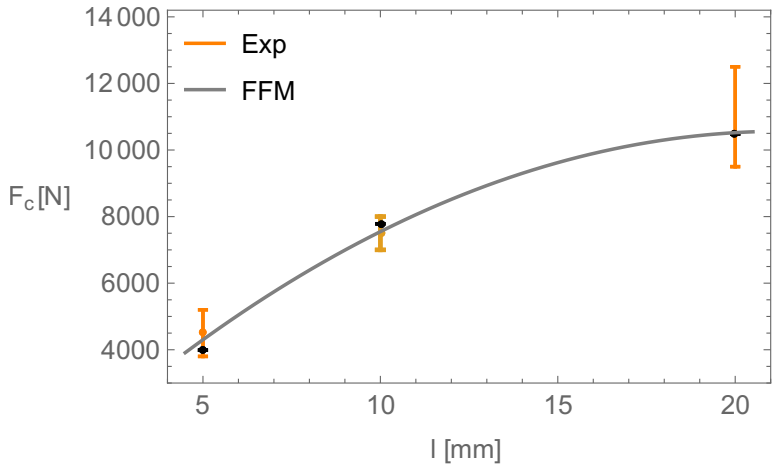

Figure 5.14: Comparison with the experimental result of the test from [2]

5.1.6 Prediction of the effective length

Considering that the problem on its own, for how as been modeled, is only dependent on three parameters: ρ, μ, λ, a prediction of the effective length (λ_{Eff}) has been performed. The effective length prediction now presented refers to maximum critical load reached with an error of the 5%. The linear relation has been evaluated by interpolating the values of the effective length at the variation of the geometrical and structural characteristics with a linear function of ρ and μ. The result found is that the λ_{Eff} can be predicted by using the following formula:

$$\lambda_{Eff} = 2.76\rho + 0.288\mu + 1.44 \tag{5.1}$$

with an average error of the 6% and a maximum error of 20%. This results holds for $\rho \in [0.1\ ,\ 1.0]$ and $\mu \in [1.0\ ,\ 12]$.
By using the same procedure, for the $\rho \in [1.0\ ,\ 1.9]$ and $\mu \in [1.0\ ,\ 12]$ the λ_{Eff} is given by the following relation:

$$\lambda_{Eff} = -2.46\rho + 0.323\mu + 6.43 \tag{5.2}$$

with an average error of the 6% and a maximum error of 15%.

5.2 Single lap joint

The single lap joint problem has been studied by using both models to find the stresses at the interface. Now it will be presented the shear lag stress model, and secondly the Goland-Reissner one. The main difference between the two solutions will be also illustrated.

5.2.1 Shear lag model

As already mentioned in Chapter 4, the average criterion has been preferred to do all the calculation for this specific case. The shape of the curve of the failure load vs. overlap length for this geometry is similar to the one of the double lap joint: it is increasing along with the overlap length until it reaches the approximate value F_c^{∞}. Due to the observation illustrated in Figure 4.3, the solution if crack propagation only on one side is supposed, is not always found by solving the equation $F_{c,e}(\delta) = F_{c,s,a}(\delta)$. Figure 5.15 shows in fact two curves, the continuous line is the solution given by solving:

$$\texttt{FindRoot}[F_{c,e}(\delta) = F_{c,s,a}(\delta),\ \delta \in [0,\ \lambda]] \tag{5.3}$$

and the dashed line is the one found by:

$$F_c = F_{c,s,a}(\delta = \lambda) \tag{5.4}$$

As it can be seen in the figure, there exists a minimum limit length λ_{lim}, for which, if the solution is searched for an overlap length below this value, it has to be used the solution of the expression 5.4, and for $\lambda > \lambda_{lim}$, the solution from 5.3. The problem just mentioned

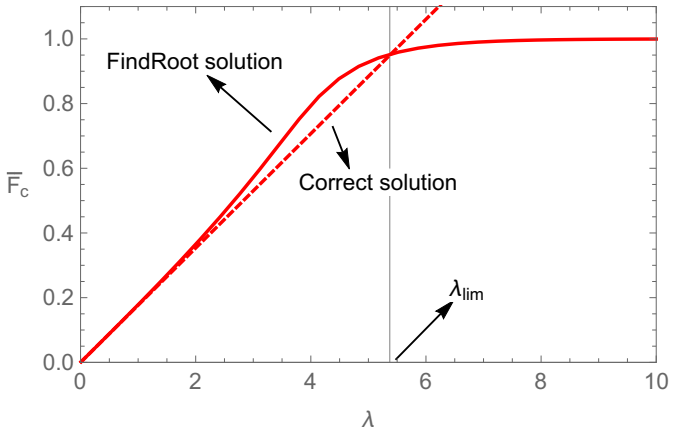

Figure 5.15: $\overline{F}_c(\lambda)$ for the single lap joint, crack propagation only on one side, $\mu = 8$.

does not exist for the case of crack propagation on both side, the solution in that case can be always found by using a `FindRoot` command. The differences between the critical load curve found with the model with propagation on one side or on both are plotted in Figure 5.16. The interval $\lambda \in [0.0,\ 10]$ has been discretizied in 50 points for obtaining the desired plot. Some observations:

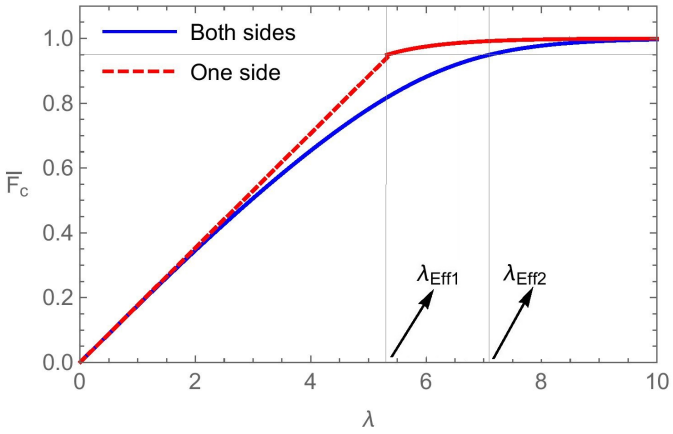

Figure 5.16: $\overline{F}_c(\lambda)$ for the single lap joint, comparison between crack propagation only on one or both sides, $\mu = 8$.

- the predicted curve with the model for propagation on both side is lower than the other one;
- the effective overlap length $\lambda_{Eff_{1,2}}$ predicted by the two models are different, the one with crack propagation on both sides is higher. The effective length prediction presented refers to maximum critical load reached with an error of the 5%;
- the time for solving both problems on a personal computer with the software Mathematica is approximately 2 seconds.

Unfortunately, this model is not really predicting the critical load in a good way due to the fact that the peeling stress at the interface cannot be disregarded in such a geometry. For this reason, the validation of the FFM solution for the single lap joint geometry will be showed by using the model from Goland-Reissner for the interface stresses.

5.2.2 Goland-Reissner model

In this section the solution provided by the Goland-Reissner model will be presented. Mainly it has been used the average shear criterion, but a comparison with Leguillon's model will also be presented. The solution for this specific case has been found by using the `NMinimize` function of the software Mathematica in the following way:

$$\begin{aligned} &\texttt{NMinimize} && F \\ &\texttt{subject to} && \texttt{energetic[F, } \Delta\texttt{]} \geq G_c \\ &&& \texttt{shear[F, } \Delta\texttt{]} \geq \sigma_c \\ &&& [\Delta, F] \in \left[[0.0, \frac{\lambda}{2}], [0.0, 100000]\right] \end{aligned}$$

In particular the function `energetic[F, Δ]` and `shear[F, Δ]` are respectively the left-hand side of the inequalities 4.18 and 4.20, that obviously are dependent on both F and Δ. The method `"RandomSearch"` has been used in order to guarantee the convergence of the solution (more information can be found on the Wolfram Language & System Documentation Center [21]). The constraints over the interval where lies the critical load have been changed depending on the material and geometrical proprieties of the single lap joint configuration studied. The study of the solution at a fixed overlap length takes approximately 3 minutes on a personal computer.

Comparison with the shear lag stress criterion

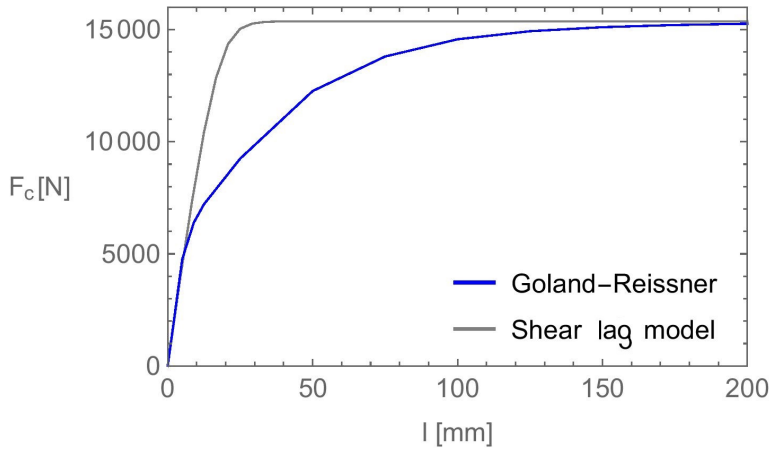

Figure 5.17: $\overline{F}_c(\lambda)$ for the single lap joint with shear lag or Goland-Reissner solution.

The comparison between the shear lag model and the Goland -Reissner one has been performed with the material and geometrical data by Da Silva et al. [7] for Steel-Redux 326-Steel single lap joints with $t = 25mm$. Figure 5.17 shows the difference of the two critical load vs. the overlap length curves.
The difference between the two models clearly shows that ignoring the peeling stresses at the interface is not a good assumption for this joint configuration. Both curves are showing the solution founded by assuming crack propagation on both sides. The curves tend to the same approximate value for an extremely long overlap length. Thus, the peel stress can be ignored only if the overlap region is sufficiently long.

Comparison between crack propagation on one or both side

The comparison of the differences between the solution by considering crack on one or both sides has been done with the same geometry used for the previous comparison (Steel-Redux 326-Steel single lap joints with $t = 25mm$ from [7]). Figure 5.18 is showing the results that have been found for the critical load the the variation of the overlap length. The difference is minimal. Only for extremely short overlap lengths the critical load obtained

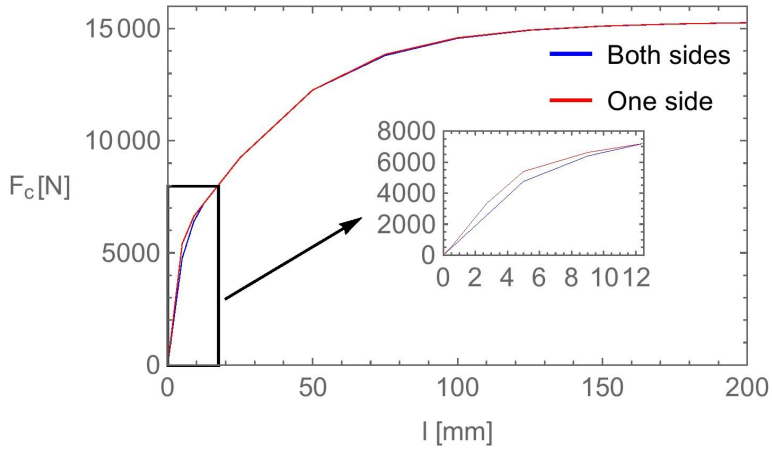

Figure 5.18: $F_c(\lambda)$ for the single lap joint with the Goland-Reissner solution by considering propagation on one or both sides. With a zoom on the curves for short overlap lengths. $\mu = 9.58$

by assuming crack propagation on both side is lower than the other one, and the difference is really small. In order to study better which criterion is more reliable in which geometric configuration, a study on the brittleness number has been performed. The brittleness number has been defined in the same way as the one in Stein et al. [18], according to the fact that the FFM approach of this work is very similar to the one used in that one. The μ parameter is thus defined as:

$$\mu = \psi \frac{E_a G_c}{h_a \sigma_c^2} \tag{5.5}$$

with

$$\psi = 2 \frac{\left(\frac{\sigma_{max}}{2} + \sqrt{(\frac{\sigma_{max}}{2})^2 + \tau_{max}^2} \right)^2}{\sigma_{max}^2 + \frac{E_a}{2G_a} \tau_{max}^2} \tag{5.6}$$

and, as for the double lap joint, this parameter relates the maximum shear stress criterion to the LEFM criterion in such a way that for a simultaneous fulfillment of these criteria, the brittleness number becomes equal to 1. The brittleness number for the model setup of Figure 5.18, is $\mu = 9.58$. In order to check if for a higher brittleness number considering crack propagation on both side gives a better solution, the same geometry of the above cited article has been used for another study, with the only difference of setting the h_a parameter equal to one half of the previous one. In this way the new results showed in Figure 5.19 considers the case of a brittleness number that is double the one just mentioned. Significant differences ($\sim 15\%$) are detected only for short overlap lengths. The difference between the two curves increases along with the brittleness index.
The reason why the geometry has not been studied for a value of the thickness of the adhesive h_a larger the one of the first result shown, it is because the hypothesis of the Goland-Reissner model do not fit well when the thickness of the adhesive is approximately

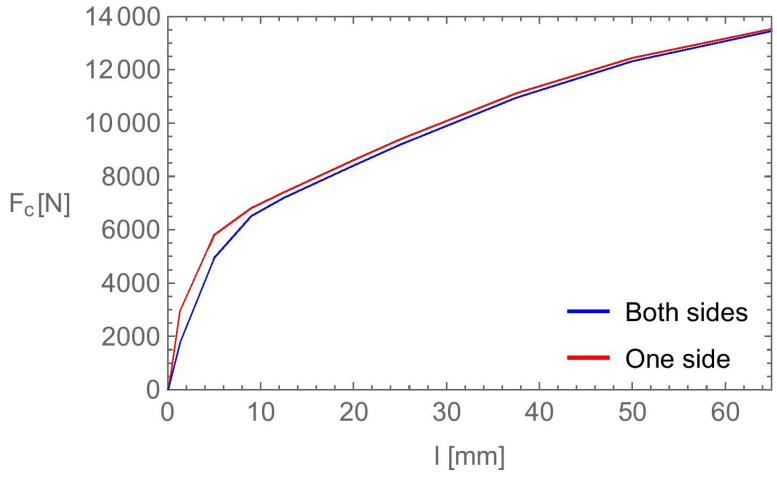

Figure 5.19: $F_c(\lambda)$ for the single lap joint with the Goland-Reissner solution by considering propagation on one or both sides. $\mu = 18.9$

equal to the one of the upper and lower block.
According to the fact that using the Goland-Reissner method is better than the shear lag one, from now on the result showed are evaluated with the Goland-Reissner solution for the interface stresses.

5.2.3 Comparison with other methods

The solution given by the finite fracture mechanic approach for the experimental setup taken from Da Silva et al. [7] for Steel-Redux 326-Steel single lap joints with $t = 25mm$, has been compared to the one given by LEFM and MSSC. The same comparison has also been done for the case of double brittleness number for analyzing better the main differences between the models, see Figure 5.21. As showed, the failure load studied with the FFM and the LEFM are almost coincident. The solution from the MSSC instead is predicting values that are lower than the ones from the other models. This result shows also some correspondences with the ones found for the double lap joint illustrated before. Moreover, if the brittleness number is increasing, there are some differences between LEFM and FFM, but only for very short overlap lengths. This observations implies that, for this specific experimental setup the results given by the more simple LEFM are predicting the failure load well.

5.2.4 Comparison with experimental results

In this section two different experimental results will be compared with the one predicted by the proposed FFM model. The first result is the one taken from the article of Da Silva et al. [7] for Steel-Redux 326-Steel single lap joints test and the other one is the test for Steel-AV138-steel from the same article both with $t = 25mm$. The material proprieties of

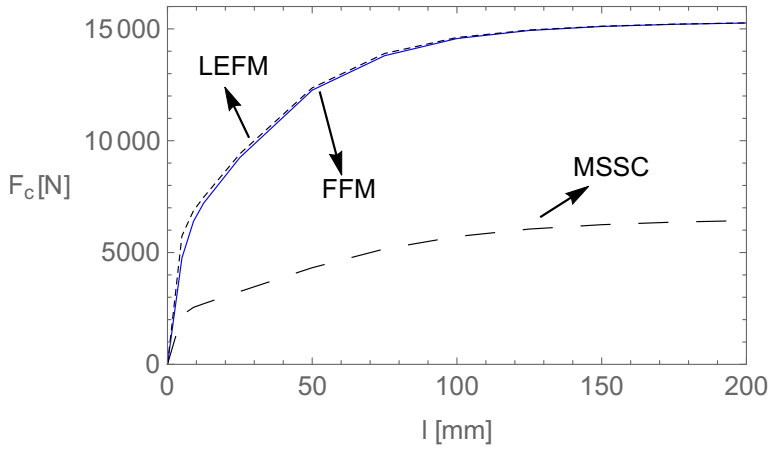

Figure 5.20: $F_c(\lambda)$ for the single lap joint with the Goland-Reissner solution by considering propagation on one or both sides. $\mu = 9.58$

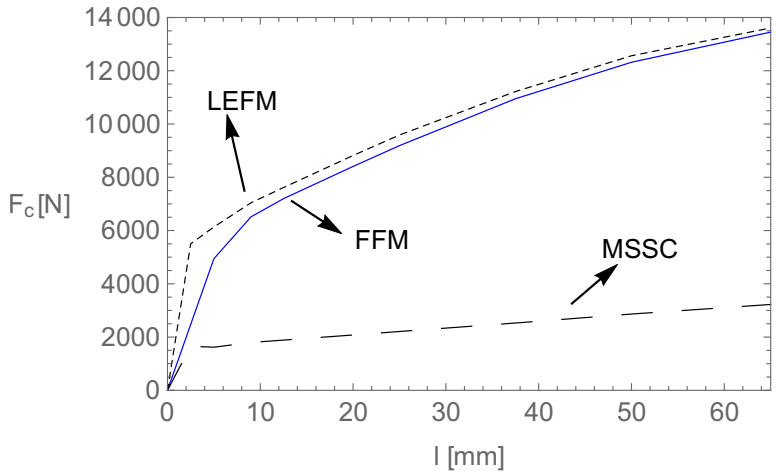

Figure 5.21: $F_c(\lambda)$ for the single lap joint with the Goland-Reissner solution by considering propagation on one or both sides. $\mu = 18.9$

both experimental tests are showed in Table 5.2.

Comparison A

The experimental test by Da Silva et al. [7] for Steel-Redux 326-Steel on single lap joints has been done for three different overlap lengths and keeping constant all the other geometric and material parameters. The comparisons are showed in Figure 5.22. The prediction from the model proposed is increasing along with the increase of the overlap region and also the value are close to the one from the experimental results.

	E_a (N/mm^2)	ν_a -	σ_c (N/mm^2)	τ_c (N/mm^2)	G_c (N/mm)	h (mm)	l (mm)	h_a (mm)
AV138	4890	0.35	39.45	30.2	0.3	2	25	*
Redux326	4440	0.35	50.9	36.6	0.3	1.5	*	0.12

Table 5.2: Parameter from the two experimental setup from da Silva et al. [7]. $E = 210GPa$ and $\nu = 0.33$ for both experiment.

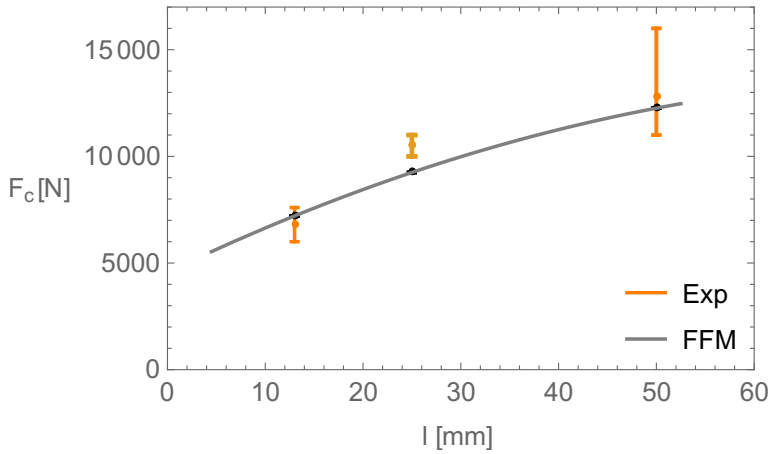

Figure 5.22: Comparison of the predicted failure loads with the experimental result from Da Silva et al.[7] for Steel-Redux 326-Steel test.

Comparison B

The other comparison proposed now is with the result by da Silva et al. [7] for the Steel-AV138-steel single lap joint. This test has been done by changing the thickness of the adhesive layer and keeping the other parameters constant. As already mentioned before, the Goland-Reissner solution is not vary accurate in case of a thickness of the adhesive similar to the one of the two block. The result is shown in Figure 5.23. As it can be seen, FFM is able to catch fairly well also the effect of the adhesive larger thickness.

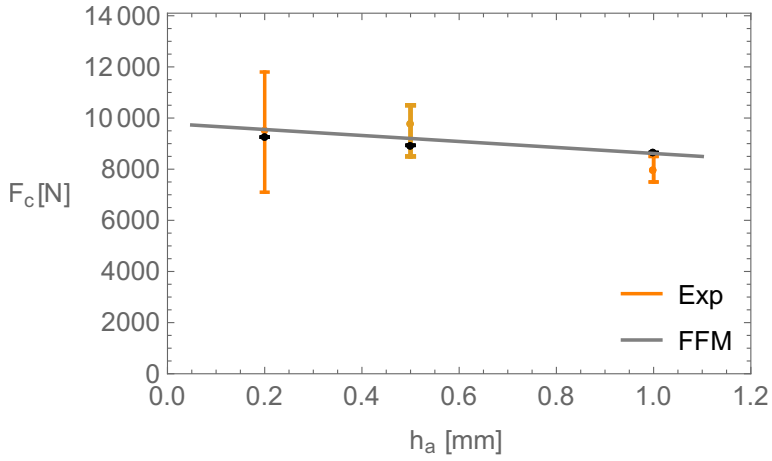

Figure 5.23: Comparison of the predicted failure loads with the experimental result from Da Silva et al. [7] for Steel-AV138-steel test.

Chapter 6

Conclusions

In this work a Finite Fracture Mechanics approach has been presented in order to predict the critical load for two specific configurations: Single and Double Lap Joint. The study, that firstly analyze the stresses at the adhesive interface, focuses on the application of a coupled stress and energy criterion. In order to validate the proposed method, a parametric analysis and a comparison with experimental data has been performed.
A deep analysis has been performed about the assumption that crack propagation starts from both extremes of the adhesive region, differently from what had already been done in other similar studies. The main conclusion is that, considering the models presented for the derivation of the interface stresses, the predicted critical load of the double lap joint configuration is more sensible to this hypothesis, while the single lap joint is less. The results show that, especially for balanced double lap joints, supposing crack propagation on both side the critical load is lower than the one predicted by assuming only on the side, i.e. where the stresses at the interface are higher. The experimental results are in agreement with the predicted ones; moreover performing the took just some seconds on a personal computer.

More in details, the studies on the Double Lap Joint showed that:

- with the proposed method the geometry can be fully described by three parameters: the non dimensional overlap length λ, the mechanical fraction of the reinforcement ρ and the brittleness number μ;
- the analysis of the critical load with respect to the parameter λ showed that after the overlap length reaches a value λ_{Eff} the critical load is approximately constant and equal to its maximum value;
- the maximum bearing load is reached faster as the overlap length increase if the mechanical fraction reinforcement ρ is lower. This implies that a geometry with a lower ρ has a lower effective length λ_{Eff};
- for a fixed overlap length the failure load is higher the lower is the brittleness number μ;

- the comparison with the results given by the LEFM and MSSC showed that for low values of μ the solution of Finite Fracture Mechanics and LEFM are mostly coincident, while at the increase of the brittleness number the Linear Elastic Fracture Mechanics is overestimating the critical load. The MSSC instead is not considered to be reliable for the prediction of the critical load according to the fact that for an infinity long overlap length the critical load is always lower than the one of the other two methods that are always in agreement;

- the comparison with the solution obtained by the Cohesive Crack Model (CCM) by Biscaia & Chastre [1], has shown that the results are in agreement especially for geometries with a low brittleness number;

- assuming crack propagation on both sides or only on one clearly shows a difference in the solution for values of ρ that are close to 1, that is when the stresses in the adhesive are mostly symmetric. In this case the results shows how the predicted failure load is lower in case the crack is propagating on both sides. Thus, neglecting double side crack propagation can lead to an overestimation;

- the comparison between the predicted failure load obtained by using the average formulation or Leguillon's formulation for the stress condition in the coupled criterion shows that the average criterion is more in agreement with the CCM solution with a linear softening cohesive law. Moreover, the failure load predicted with the point-stress method is higher with respect to the one with the average formulation. It has been preferred to use the average criterion because the solution was numerically more stable and faster;

- beside the fact that the prediction of the failure load is the goal of the presented study, looking at the crack propagation at the right and left side is also interesting. In fact, the minimum critical load that is satisfying the coupled criterion has been found for short overlap lengths when the crack is propagating on both sides even if the geometry was asymmetric and only on one side for sufficiently long overlap lengths. This can be physically explained by considering that for short overlap lengths the interaction between the two extremes is higher and playing an important role in the failure process;

- the proposed model was in agreement with the experimental results that have been considered. In particular the failure load is increasing along with the increase of the overlap length as it has also been found by experiments;

- finally a linear formula for the effective lengths λ_{Eff} has been provided. It is a function of the parameters ρ and μ.

Instead, for what concerns the geometry of the Single Lap Joint configurations, the following consideration can be done:

- two methods have been proposed for the evaluation of the stresses at the interface: one with the shear and peel stresses (Goland-Reissner) and one by only considering

the shear stress; the results clearly showed that disregarding the peel stress at the interface is not an appropriate hypothesis for this geometry;

- the provided model is only applied to symmetric configurations (i.e. the thickness of the two plates are coincident) and the model is more reliable for thin adhesive layers;
- the comparison with the results given by the LEFM, MSSC showed that for low values of the brittleness number μ the solution of Finite Fracture Mechanics and LEFM are mostly coincident, while at the increase of the brittleness number the Linear Elastic Fracture Mechanics is predicting slightly higher values of critical load but the difference is not as clear as for the Double Lap Joint configuration. Also for this configuration the MSSC is not considered to be reliable;
- a deep study has also been performed for understating how the solution is varying if the crack is supposed to develop from one or both sides and the differences are negligible. This implies that for the symmetric single lap joint geometry the finite fracture mechanic approach can be performed by considering crack only on one side;
- the comparison with the experimental results shows that the model is reliable for predicting the critical load of configurations with an adhesive thickness that is at least the half of the block thickness, while the Goland-Reissner model of the stresses at the interface is not appropriate for thicker adhesive layers.

The presented coupled criterion can be extended by taking into account the peel stresses at the interface in the model for the Double Lap Joint and studying the failure behaviour of the asymmetric Single Lap Joint geometry with a model for the stresses at the interface more complex than the Goland-Reissner one.
The author opinion is that the Finite Fracture Mechanics approach is a reliable criterion for achieving a fast and accurate prediction of the failure load for structural joints.

Appendix A

Energy balance for the double lap joint

This appendix is meant to show different methods that can be used for evaluating for the double lap joint configuration the energy balance supposing fracture on both sides. The mechanical fraction of the parameter is supposed to be $\rho \in [0.0\ ,\ 1.0]$.
The figure A.1 schematize the geometry of the problem:

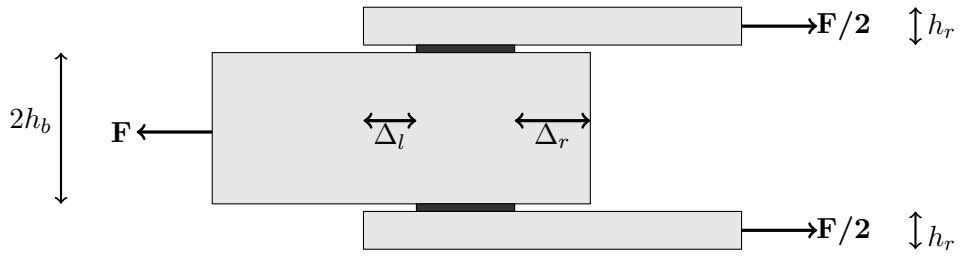

Figure A.1: Geometry of the problem

The partial energy release derived by considering when crack is propagating of $\Delta_l + \Delta_r$ only on the left or on the right side is given respectively by the equations A.1 and A.2:

$$\Delta\Phi_{p,l} = \frac{F^2}{2E_b t_b 2h_b}(\Delta_r) - 2\frac{(F/2)^2}{2E_r t_r h_r}(\Delta_r) = \frac{F^2}{4E_r t_r h_r}\Delta_r(\rho - 1)\ < 0 \tag{A.1}$$

$$\Delta\Phi_{p,r} = 2\frac{F^2}{2E_r t_r h_r}(\Delta_l) - \frac{F^2}{2E_b t_b 2h_b}(\Delta_l) = \frac{F^2}{4E_r t_r h_r}\Delta_l(1 - \rho)\ > 0 \tag{A.2}$$

And this partial expressions can be used for writing the total energy release rate in the following ways that are all equivalent:

$$\begin{aligned}
\Delta\Phi &= 2t_r \int_{l-\Delta_r}^{l} \frac{\tau_{max,r}^2(\bar{l})}{2k_t}\mathrm{d}\bar{l} + 2t_r \int_{l-\Delta_r-\Delta_l}^{l-\Delta_r} \frac{\tau_{max,l}^2(\bar{l})}{2k_t}\mathrm{d}\bar{l} \\
&= 2t_r \int_{l-\Delta_l}^{l} \frac{\tau_{max,l}^2(\bar{l})}{2k_t}\mathrm{d}\bar{l} + 2t_r \int_{l-\Delta_r-\Delta_l}^{l-\Delta_l} \frac{\tau_{max,r}^2(\bar{l})}{2k_t}\mathrm{d}\bar{l} \\
&= 2t_r \int_{l-\Delta_r-\Delta_l}^{l} \frac{\tau_{max,r}^2(\bar{l})}{2k_t}\mathrm{d}\bar{l} - \Delta\Phi_{p,r} \\
&= 2t_r \int_{l-\Delta_r-\Delta_l}^{l} \frac{\tau_{max,l}^2(\bar{l})}{2k_t}\mathrm{d}\bar{l} + \frac{F^2}{4E_r t_r h_r}\Delta_r(\rho-1)
\end{aligned}$$

The energy release can be then expressed in a non dimensional form by using the quantities introduced in the Chapter 3 and giving the following different expressions that are equivalent to the equation 3.14:

$$\begin{aligned}
&2\int_{\lambda-\delta_r}^{\lambda} \overline{\tau}_{max,r}^2(\overline{\lambda})\mathrm{d}\overline{\lambda} + 2\int_{\lambda-\delta_r-\delta_l}^{\lambda-\delta_r} \overline{\tau}_{max,l}^2(\overline{\lambda})\mathrm{d}\overline{\lambda} \\
&= 2\int_{\lambda-\delta_l}^{\lambda} \overline{\tau}_{max,l}^2(\overline{\lambda})\mathrm{d}\overline{\lambda} + 2\int_{\lambda-\delta_r-\delta_l}^{\lambda-\delta_l} \overline{\tau}_{max,r}^2(\overline{\lambda})\mathrm{d}\overline{\lambda} \\
&= 2\int_{\lambda-\delta_r-\delta_l}^{\lambda} \overline{\tau}_{max,r}^2(\overline{\lambda})\mathrm{d}\overline{\lambda} - \overline{F}^2 2\mu\delta_l(1-\rho^2) \\
&= 2\int_{\lambda-\delta_r-\delta_l}^{\lambda} \overline{\tau}_{max,l}^2(\overline{\lambda})\mathrm{d}\overline{\lambda} + \overline{F}^2 2\mu\delta_r(1-\rho^2) \\
&= \frac{2k_t G_c}{\tau_c^2}(\delta_r+\delta_l)
\end{aligned}$$

Appendix B

Observations on the mechanical fraction of the reinforcement parameter for the double lap joint

This appendix is meant to show the main differences that have to be considered if the mechanical fraction of the reinforcement ρ is greater than 1 for the double lap joint configuration. The definition of the parameter is given by:

$$\rho = \frac{E_r t_r h_r}{E_b t_b h_b}.$$

By noticing that, for $\rho > 1$, the absolute maximum of the shear stress at the interface (equation 3.7) is on the left side of the geometry showed in the figure 3.1, the following expression have to be considered that the failure load for infinite overlap length is:

$$F^{\infty}_{c,\rho>1} = \frac{2t_r}{\rho}\sqrt{2(1+\rho)E_r h_r G_c}$$

with:

$$\overline{\tau} = \frac{\tau}{\tau_c}, \quad \overline{F}_{\rho>1} = \frac{F}{F^{\infty}_{c,\rho>1}},$$

and:

$$\overline{\tau} = \overline{F}_{\rho>1}\sqrt{\mu}\ \frac{\cosh(\lambda-\xi)+\frac{1}{\rho}\ \cosh(\xi)}{\sinh(\lambda)}.$$

Note that, at the variation of the parameter ρ, the maximum F^{∞}_c is found for $\rho = 1$. The figure B.1 shows the profile of the $F^{\infty}_c(\rho)$ for some selected geometrical and material parameters.

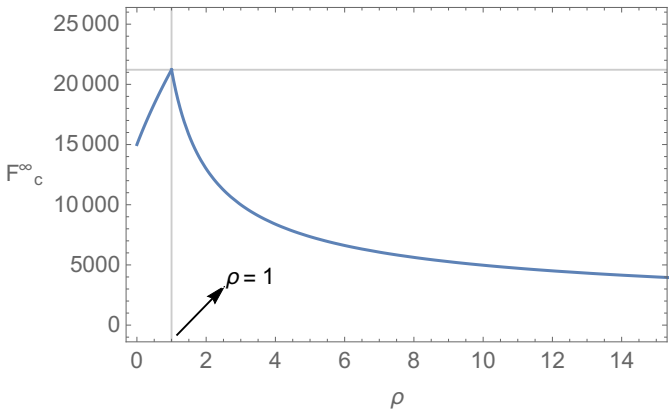

Figure B.1: Plot of the function $F_c^{\infty}(\rho)$ for $t_r = 12.5mm$, $h_r = 3mm$, $E_r = 200GPa$ and $G_c = 0.3N/mm$.

Bibliography

[1] H. C. Biscaia and C Chastre. "Theoretical analysis of fracture in double overlap bonded joints with FRP composites and thin steel plates". In: *Engineering Fracture Mechanics* 190 (2018), pp. 435–460.

[2] R.D.S.G. Campilho and M.D. Banea A.M.G. Pinto L.F.M. Da Silva A.M.P. de Jesus. "Strength prediction of single- and double-lap joints by standard and extended finite element modelling". In: *International Journal of Adhesion and Adhesives* 31.5 (2011), pp. 363–372.

[3] C. S. Chen D. "An Analysis of Adhesive-Bonded Single-Lap Joints". In: *Journal of Applied Mechanics* 50 (1983), pp. 109–115.

[4] P. Cornetti, N. Pugno A. Carpinteri, and D. Taylor. "Finite fracture mechanics: A coupled stress and energy failure criterion". In: *Engineering Fracture Mechanics* 73.14 (2006), pp. 2021–2033.

[5] P. Cornetti, V. Mantič, and A. Carpinteri. "Finite Fracture Mechanics at elastic interfaces". In: *International Journal of Solids and Structures* 49.7-8 (2012), pp. 1022–1032.

[6] P. Cornetti, A. Sapora, and A. Carpinteri. "Short cracks and V-notches: Finite Fracture Mechanics vs. Cohesive Crack Model". In: *Engineering Fracture Mechanics* 168 (2016), pp. 2–12.

[7] L. F. M. Da Silva, T. N. S. S. Rodrigues, and M. A. V. Figueiredo M. F. S. F. De Moura J. A. G. Chousal J. A. G. "Effect of Adhesive Type and Thickness on the Lap Shear Strength". In: *The Journal of Adhesion* 82.11 (2006), pp. 1091–1115.

[8] M. Goland and E. Reissner. "Stresses in cemented joints". eng. In: *Journal of Applied Mechanics* 11 (1944), A17–A27.

[9] A. A. Griffith. "The phenomena of rupture and flow in solids". In: *Philosophical Transactions of the Royal Society of London. Series A, containing papers of mathematical or physics character* 221 (1921), pp. 163–198.

[10] A. Hillerberg, M. Modéer, and P. Petersson. "Analysis of crack formation and crack growth in concrete by means of fracture mechanics and finite elements". In: *Cement And Concrete Research* 6.6 (1976), pp. 773–782.

[11] C.E. Inglis. "Stresses in a plate due to the presence of cracks and sharp corners". In: *Trans. Inst. Nav. Archit. London 55* (1913), pp. 219–230.

[12] G. R. Irwin. “Analysis of stresses and strains near the end of a crack traversing a plate”. In: *Journal Applied Mechanics* E24 (1957), pp. 351–369.

[13] K.B. Katnam, L.F.M. Da Silva, and T.M. Young. “Bonded repair of composite aircraft structures: A review of scientific challenges and opportunities”. In: *Progress in Aerospace Sciences* 61.C (2013), pp. 26–42.

[14] D. Leguillon. “Strength or toughness? A criterion for crack onset at a notch”. In: *European Journal of Mechanics / A Solids* 21.1 (2002), pp. 61–72.

[15] L. Mendoza-Navarro, A. Diaz-Diaz R. Castaa-Eda-Balderas S. Hunkeler, and R. Noret. “Interfacial failure in adhesive joints: Experiments and predictions”. In: *International Journal of Adhesion and Adhesives* 44 (2013), pp. 36–47.

[16] V.V. Novozhilov. “On a necessary and sufficient criterion for brittle strength”. In: *Journal of Applied Mathematics and Mechanics* 33.2 (1969), pp. 201–210.

[17] Lenci S. “Analysis of a crack at a weak interface”. In: *International Journal of Fracture* 108 (2001), pp. 275–290.

[18] N. Stein, P. Weißgraeber, and W. Becker. “A model for brittle failure in adhesive lap joints of arbitrary joint configuration”. In: *Composite Structures* 133.C (2015), pp. 707–718.

[19] P. Weißgraeber and W. Becker. “Finite Fracture Mechanics model for mixed mode fracture in adhesive joints”. In: *International Journal of Solids and Structures* 50 (2013), pp. 2383–2394.

[20] M. L. Williams. “Stress singularities resulting from various boundary conditions in angular corners of plates in extension”. In: *Journal of Applied Mechanics* 19 (1952), 526–528.

[21] *Wolfram Language System Documentation Center*. http://reference.wolfram.com/language/. Accessed: 2018-06-30.